



POLITECNICO DI TORINO

Master of Science in Biomedical Engineering

MASTER OF SCIENCE THESIS

Thesis in the Company Eltek S.p.A

***Cell impedance measurements through a double approach: M4N
and litho-fabricated microelectrodes and microfluidics.***

Tutors

Prof. Danilo Demarchi

Dott. Marco Pizzi

Dott. Alessandro Sanginario

Candidate

Susana Fuentes Vélez

July 2018



POLITECNICO DI TORINO

Laurea Magistrale in Ingegneria Biomedica

TESI DI LAUREA MAGISTRALE

Tesi in azienda: Eltek S.p.A

***Misure di impedenza su cellule mediante un duplice approccio: M4N
e dispositivi microfluidici e microelettrodi.***

Relatori

Prof. Danilo Demarchi

Dott. Marco Pizzi

Candidato

Susana Fuentes Vélez

Correlatori

Dott. Alessandro Sanginario

Luglio 2018

Desidero ringraziare il Prof. Demarchi e il Dott. Pizzi per avere reso possibile lo svolgimento di questa tesi. Grazie per l'opportunità, la disponibilità, la guida e la fiducia concessa durante lo svolgimento della tesi.

Ringrazio il Dott. Sanginario per la sua disponibilità, suggerimenti, collaborazione e pazienza.

Ringrazio la Dott.ssa Beatrice Miccoli per introdurmi al progetto del M4N.

Ringrazio Barbara e Flori del Dipartimento di Fisica dell'Università di Torino per la loro preziosa collaborazione, pazienza e disponibilità.

Ringrazio il personale della Eltek S.p.A, specialmente ai colleghi di laboratorio che mi hanno aiutato nel lavoro quotidiano con pazienza e cortesia, e per rendere di grandissimo valore la mia esperienza in azienda.

Grazie a tutti gli amici in Colombia e in Italia che mi hanno supportato in questo percorso.

Un grazie, inoltre, alla mia famiglia per il supporto incondizionato che ha reso tutto questo possibile.

A mi familia, que hizo todo esto posible.

Abstract

Within the frame of biomedical research and specifically taking advantage of the multiple possibilities of experimentation opened by the synergy between electronics and biology, emerges the present work. The following is an experimental thesis developed in collaboration between **Politecnico di Torino** and the Company **Eltek S.p.A** (Hone, Valle D'Aosta, Italia headquarters).

This work is motivated by the advantages that going to the *micro* and the *nano*-scale can offer to cell biology for applications in health and environmental sciences. To do so, many challenges turn up in areas such as microelectronics and microfluidics. In this thesis, the subject is approached focusing on impedance measurement analysis. Using impedance changes as an indicator provides the advantages of a label-free technique with a high scalability potential.

Two main experimental projects are proposed. The first one is the M4N characterization in aqueous environment. It is motivated by the aim of inquiring the potential of this multisensory platform for bio-sensing applications. This part was specifically directed towards a proof of concept on cell impedance measurement. Experiments were conducted with yeast cells and a preliminary study of the M4N as a gas sensing platform is also presented. The second project consists on microelectrodes fabrication through photolithographic techniques and their successive integration with microchannels for cell impedance measurement purposes. Different configurations of electrodes and microchannels are presented. Tests were conducted with yeast cells and a direct relation between concentration and impedance was observed. Impedance measurements in microchannels with interdigitated microelectrodes, in contrast to analog measurements in culture wells, showed to solve the problem of aggregates formation on the electrode surface, showed enhanced sensibility, and showed reduction in measuring time and sample volumes. Impedance was measured with two different instruments: a commercial impedance-meter and an acquisition system designed and developed at the Company **Eltek S.p.A**.

Contents

Introduction.....	9
Motivation.....	11
1. Chapter I – M4N Overview	13
1.1 A multipurpose CMOS platform for Nanosensing	13
1.1.1 Nanostructured element integration	13
1.1.2 Read Out System	13
1.2 The M4N approach overview	14
1.3 M4N Fabrication.....	16
1.4 Dielectrophoresis (DEP).....	17
1.5 Read-out circuits (ROC).....	18
1.5.1 The two-quadrants quasi-digital impedance converter (QDIC)...	19
1.5.2 Calibration and measurement	20
1.6 Electronic interface	21
2. Chapter II – Microelectrodes and Microchannels.....	24
2.1 Overview on microfabrication technologies	24
2.1.1 Basic methods	25
2.1.2 Advanced methods.....	26
2.2 Microfabrication by Photolithography	27
2.2.1 Output assessment: profilometry.....	28
3. Chapter III –Cell impedance measurement	30
3.1 Electric model of a single cell	30
3.2 Cell impedance measurement techniques.....	32
3.2.1 Yeast cells and impedance measurement	33
3.3 Microfluidic Chips for cell impedance measurement.....	34
4. Chapter IV – M4N Experimental part.....	35
4.1 M4N Chip assembly.....	35
4.1.1 Experimental design: material and methods	35
4.1.2 Results and discussion.....	36

4.2	M4N calibration	38
4.2.1	Experimental design: material and methods	38
4.2.2	Results and discussion.....	39
4.3	M4N characterization in aqueous environment	41
4.3.1	Experimental design: material and methods	42
4.3.2	Results and discussion.....	43
5	Chapter V – Microelectrodes and Microchannels Experimental part.....	52
5.1	Microelectrodes fabrication.....	52
5.1.1	Experimental design: material and methods	52
5.1.2	Results and discussion.....	54
5.2	Microchannels fabrication.....	57
5.2.1	Experimental design: material and methods	57
5.2.2	Results and discussion.....	59
5.3	Microelectrodes-microchannels integration and impedance measurement.....	61
5.3.1	Experimental design: material and methods	61
5.3.2	Results and discussion.....	62
	Conclusions and future perspectives.....	74
A.	Figures Index	76
B.	Tables Index.....	80
	Bibliography	81

Introduction

Biomedical research is a continuously growing field thanks to its potential to improve life's quality. It is a multidisciplinary area in which there will always be challenges to overcome.

The synergy between electronics and biology has opened a range of possibilities and applications both in health and environmental sciences. Additionally, the several advantages of working on the microscale have led to developments on both microelectronics and microfluidics that match the required characteristics of cell biology. Microelectronics and microfluidics have therefore found several applications in cell biology: cancer research, drug screening, point-of-care and point-of-need diagnosis devices, and food and environmental monitoring, among others [1].

State-of-the-art and emerging microfabrication technologies are thought to have the potential to generate a whole new generation of biosensors and integrated platforms able to change the actual healthcare paradigm. Miniaturized biosensing systems have several advantages, among the most named: portability and cost-effectiveness [2]. Specifically, CMOS¹ technologies have proved to be a plausible approach for biosensing applications. Among them, *in vitro* diagnosis is a widely studied subject [3].

In the following thesis, the subjects CMOS platforms for biosensing, microfluidics, and microelectronics will be addressed. The thesis reports two main research projects developed in collaboration between **Politecnico di Torino** and the Company **Eltek S.p.A.**, (Hone, Valle D'Aosta, Italia headquarters).

The first project is related to the "Micro-for-Nano (M4N)" chip developed by **Bonanno. A.** at **Politecnico di Torino**, while the second one is related to microelectrodes and microfluidics and takes advantage of the lithographic processes and equipment of the Company **Eltek S.p.A.** They are both related by their target experimental application: cell impedance measurement.

The first two chapters stand for the State-of-the-art of the two methodologies used for measurement and analysis. **Chapter I** presents an overview of the M4N system. **Chapter II** is a theoretical background on microelectrodes fabrication and

¹ CMOS: Complementary metal oxide semiconductor.

microfluidics. Then, a State-of-the-art on cell impedance measurement is presented in **Chapter III**.

Following chapters explain experimental procedures and present qualitative and quantitative results with their respective analysis and discussion. **Chapter IV** reports the performed tests with the M4N and **Chapter V** contains the followed procedure for microelectrodes and microchannels fabrication and experimental tests results. Experimental chapters are presented in a simplified structure in which for each experiment, first the objective is identified, then experimental design is explained (materials and methods), and finally, results and discussion are presented.

At the end, from the literature review and the experimental results, conclusions and future perspectives are formulated.

Motivation

Biosensing, and particularly microdevices to do so, are of general and growing interest in biomedical research because, from a global point of view, they have the potential to impact public health and, as mentioned in the introduction, it is even thought that they are able to change the actual healthcare paradigm.

On the report of the “Bioelectronics Roundtable” held in North Carolina and published on February 2009, the topics disease detection and prevention, Lab-on-Chip and nanofabrication are mentioned, among others, as “highest priority topics” [1].

In *Figure 0.1* is presented the number of publications per year in the last 20 years by searching: “*biosensing AND cells AND impedance*” in the ELSEVIER’s database *Scopus*. The overall increase among the years makes evident the growing interesting on the subject [4].

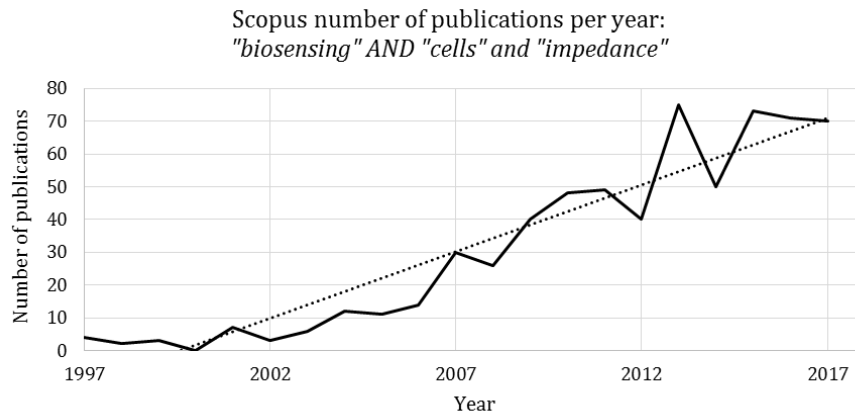


Figure 0.1. Scopus publications per year about “biosensing AND cells AND Impedance”. [4].

The present work is motivated by the numerous advantages that going to the Micro and Nano-scale provide to cell biology. The experimentation is directed to bring together microelectronics and microfluidics in a way that matches the required characteristics for a useful cell impedance measurement with potential applications in health and environmental sciences. The potential of measuring cell impedance consists on the information that it can give about the cell membrane or the cytoplasm and that can be correlated with physiological or pathological

changes. Direct applications include cytometry, cell viability, cell vitality, cell type discrimination and drug screening.

Downscaling is the scope. Going closer to the cellular dimensions, both with the fluidics and the electronics, opens the possibility for more significant and sensible measurements. On the other hand, it is advantageous from the industrial point of view because of its potentially enhanced cost-effectiveness.

With the downscaling objective and with cell impedance measurement as the target application, two approaches were studied: M4N and litho-fabricated microelectrodes and microfluidics. Each of the approaches presented different challenges.

The M4N experimental part was also motivated by the will of giving continuity to the M4N project and to exploit the potential of this integrated multisensory platform. Features such as integrated microelectronics (already optimized for parasitics reduction and low-noise measurement), interface with commercial electronics (Arduino Due), implemented graphic user interface (GUI) for real-time acquisition and multi-nanosensor capability, makes it attractive for multiple bio-sensing applications. A characterization of the system in aqueous environment and a validation of the ROCs² for cell impedance measurement was needed. First steps towards a proof of concept and further experimentations on the potentiality of the M4N towards a so-called “Cell-on-Chip” were performed.

Litho-fabricated microelectrodes and microfluidics experimental part was motivated by the need of optimizing the impedance measurement set-up. By set-up is intended the whole system configuration going from microelectrodes and microfluidics fabrication and integration, passing through impedance read-out, data acquisition, processing, and arriving to interpretation and data analysis. The know-how and equipment present in the company were used for these purposes.

² ROC: Read Out Circuits

1. Chapter I – M4N Overview

1.1 A multipurpose CMOS platform for Nanosensing

Nanosensors research and development is a growing field and constitute the basis of a new generation of devices with promising features [5]. The use of nanostructured materials, like nanowires, nanoparticles or thin films, able to interact with molecules, gases or bio-substances at the nanoscale, opens the door to a whole new area of bio-sensing applications. Specifically, the use of a single nanostructured element present several advantages such as the dimension reduction and the improved sensitivity and accuracy [6].

There are two main issues to be addressed when talking about nanosensors: the integration of the nanostructured element with the electrodes, and the electronic interface or read-out system. A CMOS platform allows the design and implementation of low-power and low-noise custom circuits for high accuracy measurements with low-cost mass production and technology scale-down [7].

1.1.1 Nanostructured element integration

Since the nanomaterial is the sensing element, it should be exposed to the external environment and therefore its integration with the CMOS platform takes place using a “post-processing” technique. Most used methodologies reported in literature can be classified in two groups: deposition upon interdigitated electrodes using micromanipulator probes, direct growth of nanomaterials *in-situ* using seeds or self-assembly monolayers (SAM), and electrically controlled deposition of nanomaterials in liquid solution (like Focus Ion Beam Deposition, 3D inkjet printing of conducting material and Dielectrophoresis) [6].

1.1.2 Read Out System

Fundamentally, what is measured is the resistance or capacitance variation of the nanomaterial that is proportional to the sensed quantity. The electronic interface should be able to measure in the required range, overcome parasitic, coupling and

flicker noise, and convert the variation into signals (analog or digital) compatible with commercial electronics [8].

Moreover, both to produce reliable results and to open the possibility of a multi-purpose measurement system, an array of nanosensors, instead of a single one, should be considered [6].

1.2 The M4N approach overview

The M4N approach conceived and developed by *Bonanno. A* [6] as “a low power platform for nanomaterial integration and nanosensors interface on 0.13 μm CMOS technology” is a System-on-Chip (SoC) that integrates an array of nanowires on top of Aluminium Top Electrodes (ALTEs) that connected to a microcontroller allows real-time data acquisition and processing [6]. Its capability to integrate nanomaterials on top of a silicon chip leads to several advantages such as parasitics reduction and low-noise measurement [8].

The current version of the M4N Chip follows the multi-electrode array (MEA) topology and it is formed by 8 elements or “systems-on-chip” (SoC). Each element is composed of three couples of ALTEs, 3 quasi-digital Read-Out Circuits (ROCs) and a Dielectrophoresis (DEP) generator. As each one of the elements can be individually configured, the M4N chip allows up to 8 different experiments even with 8 different types of NWs³. This important feature makes the M4N an integrated multisensory platform[5]. The distance between the three couples of ALTEs is 2.5 μm , 7.5 μm and 10 μm [9].

The ROCs are oscillator-based circuits that produce a quasi-digital signal output. The 24 outputs are multiplexed sending 3 signals at the time to the microcontroller. The M4N chip is interfaced with commercial electronics with an Arduino Due that allows real-time measurements visualization by serial communication with a GUI (graphic user interface) [6]. *Figure 1.1* is a picture of the entire M4N System and *Table 1.1* is an overview of M4N main features.

³ NWs: Nanowires

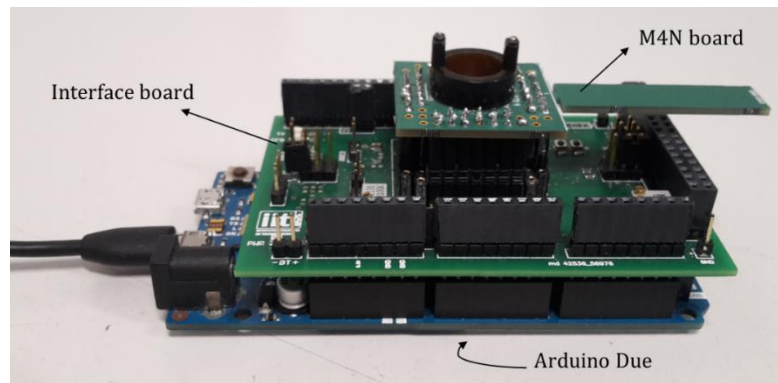


Figure 1.1. M4N complete system.

M4N Features	
CMOS Technology	0.13 μm
Silicon chip area	1.2 mm x 1.2 mm
SoC area	0.02 mm ²
Theoretic integration factor	150 nanosensors/mm ²
SNR	47 dB (@ C=47pF)
Power consumption	14.82 μW
Interfacing semiconductive nanosensors	
R-Range	1M Ω - 1G Ω
C-Range	0 - 100 pF
Circuits	
ROC	Supply voltage: 1.2 V
	AC triangular signal
	Frequency range: kHz
	V _{pp} =120 mV
	V _{dc} =710 mV
DEP circuit	Supply voltage: 3.3 V
	AC triangular wave
	Maximum frequency: 50 kHz - 1 MHz
	I _{bias} = 5 μA - 25 μA

Table 1.1. Overview of the M4N main features.

1.3 M4N Fabrication

In *Figure 1.2* the whole fabrication process is illustrated.

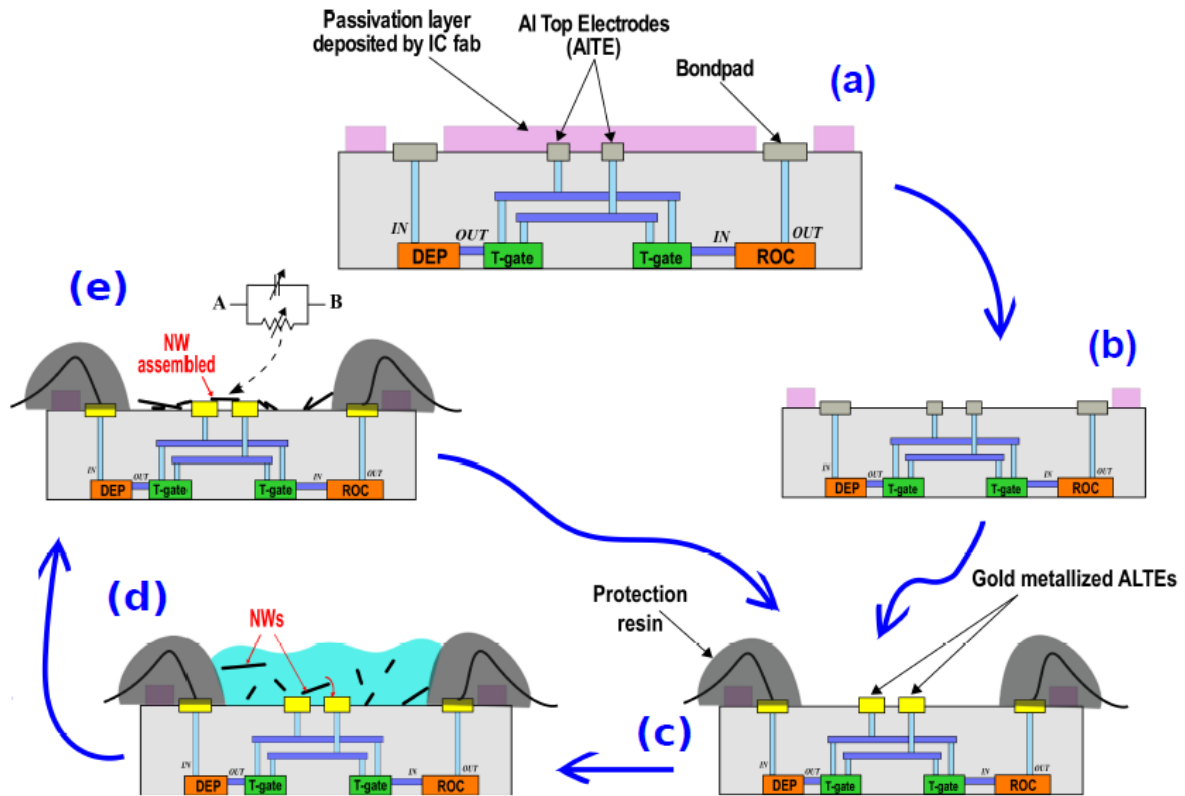


Figure 1.2. M4N fabrication flow (Figure from [5]).

Main steps presented in *Figure 1.2* are explained in detail as follows:

- a) M4N chips are fabricated using standard 130nm CMOS technology in a Multi- Project Wafer and passivation layer of Silicon Nitride (Si_3N_4) and Phosphosilicate Glass (PSG) is deposited on the chip surface during the silicon fabrication process for protection.
- b) The first post-processing step is to expose the AlTEs for the subsequent nanomaterial deposition. The removal of this passivation layer is done by means of Reactive Ion Etching (RIE). RIE is done with a RIE STS 320 machine and a SF_6 gas to which the aluminum acts as a stop etch layer.
- c) To avoid electrodes oxidation, a metallization with gold can be performed. The metallization proposed process consists of an electroless plating based on chemical reactions.
- d) The M4N chip is bonded and then an insulating resin is deposited for bond-wire protection.
- e) NWs are deposited by dielectrophoresis (DEP) [5].

1.4 Dielectrophoresis (DEP)

DEP is the physical phenomenon that determines the translational motion of a particle under a spatially non-uniform electric field. It depends on permittivity, conductivity, and dielectric properties. *Equation 1.1* defines the DEP force for a homogeneous spherical particle [10].

$$F_{DEP} = 2\pi\epsilon_m R^3 \operatorname{Re}[K_i(\omega)] |E| \cdot \nabla |E| \quad \text{Equation 1.1}$$

ϵ_m : Permittivity of the medium surrounding the particle.

R : Radius of the particle.

$K_i(\omega)$: Clausius-Mossotti factor (ω : frequency)

E : Electric field

The direction of the particle translation depends on the Clausius-Mossotti factor (*Equation 1.2*). This factor expresses the frequency-dependent difference between the complex permittivity of the particle and the surrounding media: particles more polarizable than their surrounding are attracted to where the field is higher by positive DEP (pDEP) and, in the opposite case, particles are moved away from the high field region by negative DEP (nDEP) [10].

$$K_i(\omega) = \left[\frac{\epsilon_p^* - \epsilon_m^*}{\epsilon_p^* + 2\epsilon_m^*} \right] \quad \text{Equation 1.2}$$

ϵ_p^* : Complex permittivity of the particle

ϵ_m^* : Complex permittivity of the medium

Complex permittivity is defined as follows [10]:

$$\epsilon^* = \epsilon + \frac{\sigma}{j\omega} \quad \text{Equation 1.3}$$

σ : Conductivity

In the M4N the methodology implemented for nanostructured material integration in the M4N approach is the Dielectrophoresis (DEP). It is a fast, widely diffused, and a low-cost technique in which the application of an alternating electric field gradient between two electrodes attracts and orients nanostructured materials suspended in solution. Polar nano-wires with lengths comparable to the gap between the electrodes can be positioned by means of this technique following the electric field lines (*Figure 1.3*) [6].

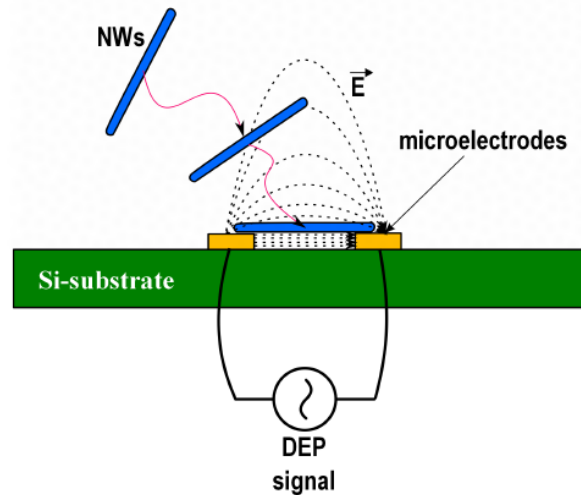


Figure 1.3. Schematic representation of NWs alignment by DEP (Figure from [6]).

1.5 Read-out circuits (ROC)

As well described by *Bonanno. A* [6], ROCs for nanosensors have several design constraints in terms of power consumption and silicon area. The M4N system integrates quasi-digital, low power, small-size ROCs that allow real-time and parallel acquisition. They are based on oscillators that with a low-complexity architecture produce a 1-bit-quasi-digital output signal.

A simplified electric representation of a nanomaterial is a resistance (R_{nano}) parallel to a capacitance (C_{nano}). The quasi-digital approach implies the conversion of these quantities into the time domain producing an output signal modulated in frequency or in duty-cycle. This output signal is then processed by a time-to-digital converter obtaining a standard N-bit representation. Main advantages of using a quasi-digital converter are good SNR, large input dynamic range, low power consumption, small silicon area, high noise immunity and easy technology scaling [9].

Semiconductor NWs can have an asymmetric V-I curve. This means that their sensibility is different according to the polarity of the stimulation signal. Since DEP deposition of NWs does not give information about the NWs orientation, the ROC implemented in the M4N system is a two-quadrants quasi-digital impedance converter that allows the measurement of nanomaterial's resistance and capacitance in the first and third quadrant separately [9].

1.5.1 The two-quadrants quasi-digital impedance converter (QDIC)

The M4N implemented QDIC is represented in *Figure 1.4* and consists of a digitally controlled relaxation oscillator that applies an AC signal to the single NWs and reads out the impedance variation. The applied signal is a triangular-wave in the kHz range with $V_{pp}=120\text{mV}$ and a DC offset $V_{DC}=710\text{mV}$.

MUX1 and **MUX2** switch the AC signal polarity that is determined by the digital signal *sel*. If *sel* is “1”, node B is grounded and V_{AB} is positive. The *out* signal is “0” for time T_0 and “1” for time T_1 . The capacitance C_{INT} represents an integrated capacitor of 5pF. C_{INT} and C_{NW} are charged through transistors **Mp1** or **Mp2** during T_0 and discharged through R_{NW} during the rest of the oscillation period. This way T_0 encodes C_{NW} while T_1 is proportional both to C_{NW} and R_{NW} . This ROC output is then processed by a time-to-digital converter, after a microcontroller calculates average and standard variation values of T_0 and T_1 and finally, using the equation that will be described in *Section 1.5.2*, the correspondent values of C_{NW} and R_{NW} are estimated[6], [9].

Mp3 and **Mp4** serve as partial leakage compensation. This is crucial because leakage currents of **Mn1**, **Mn2** and **MUX2** allow C_{INT} to be discharged even in absence of NWs, limiting, therefore, the dynamic input range [6], [9].

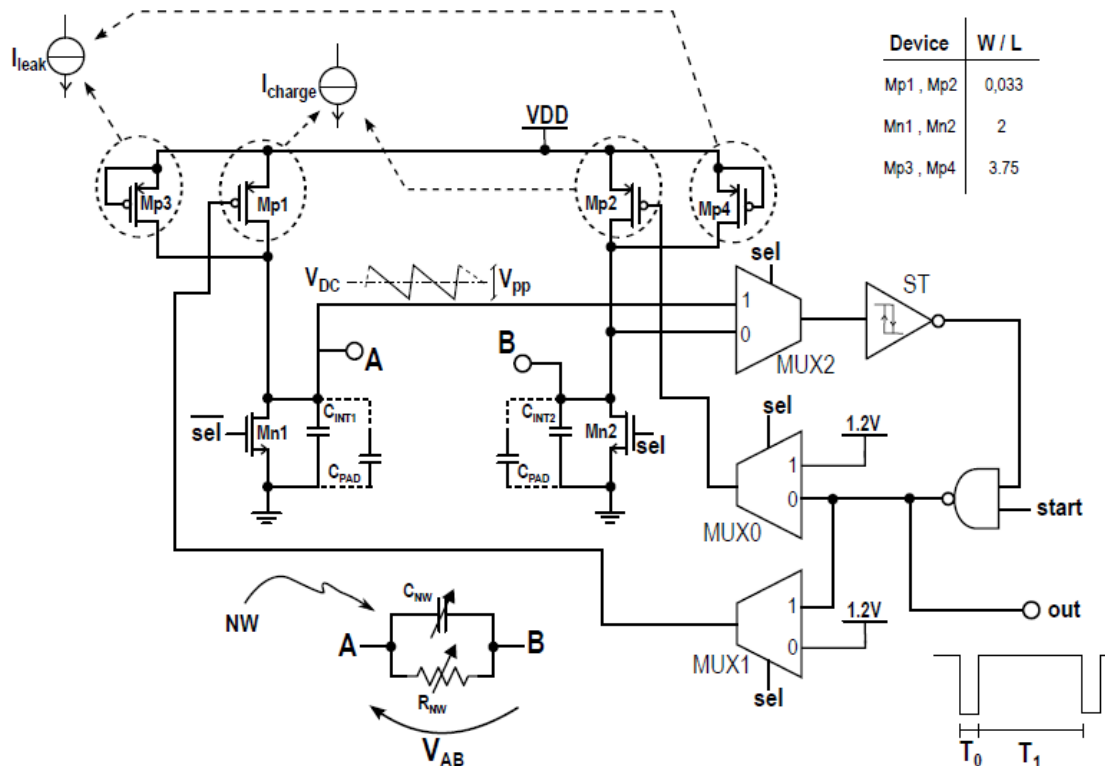


Figure 1.4. Schematic of the Quasi-Digital Impedance Converter (QDIC) (Figure from [9]).

1.5.2 Calibration and measurement

For the ROC characterization, there is a couple of electrodes A and B that are directly connected to the output PAD's. Assuming B grounded (*sel* is "1"), when no load is connected to A, the output is due to a parasitic resistance and a basal capacity for the electrode connected to the pad is defined as:

$$C_{base} = C_{INT} + C_{PAD} \quad \text{Equation 1.4}$$

C_{base} can be calculated by knowing T_0 and the ROC sensitivity ($\Delta C/\Delta T_0$). To do so, a known capacitor (C_{add}) is temporarily connected to A, perturbing the value of T_0 to T_0' . Then assuming $\Delta T_0=(T_0'-T_0)$ and $C=C_{add}$, the expression for C_{base} calculation becomes:

$$C_{base} = T_0 \frac{C_{add}}{(T_0'-T_0)} = T_0 \frac{\Delta C}{\Delta T_0} \quad \text{Equation 1.5}$$

R_{par} is defined as:

$$R_{par} = a \frac{T_1}{C_{base}} \quad \text{Equation 1.6}$$

Where "a" is a calibration parameter defined by the edges of the hysteresis gap of the Schmitt Trigger (ST).

The procedure is similar when a load (e.g. Nanowire) is connected. Assuming $C_{TOT}=C_{base}+C_{load}$ and the equivalent resistance $R_{eq}= R_{par} || R_{load}$, then C_{load} and R_{load} can be calculated as:

$$C_{load} = T_{0load} \frac{C_{add}}{(T_{0load}'-T_{0load})} - C_{base} = T_{0load} \frac{\Delta C}{\Delta T_0} - C_{base} \quad \text{Equation 1.7}$$

$$R_{load} = \frac{a * T_{1load} * R_{par}}{(C_{TOT} * R_{par}) - (a * T_{1load})} \quad \text{Equation 1.8}$$

Bonano's proposed "Two-steps Algorithm for Circuit Calibration" is summarized in the flow diagram of Figure 1.5 [6], [9], [11].

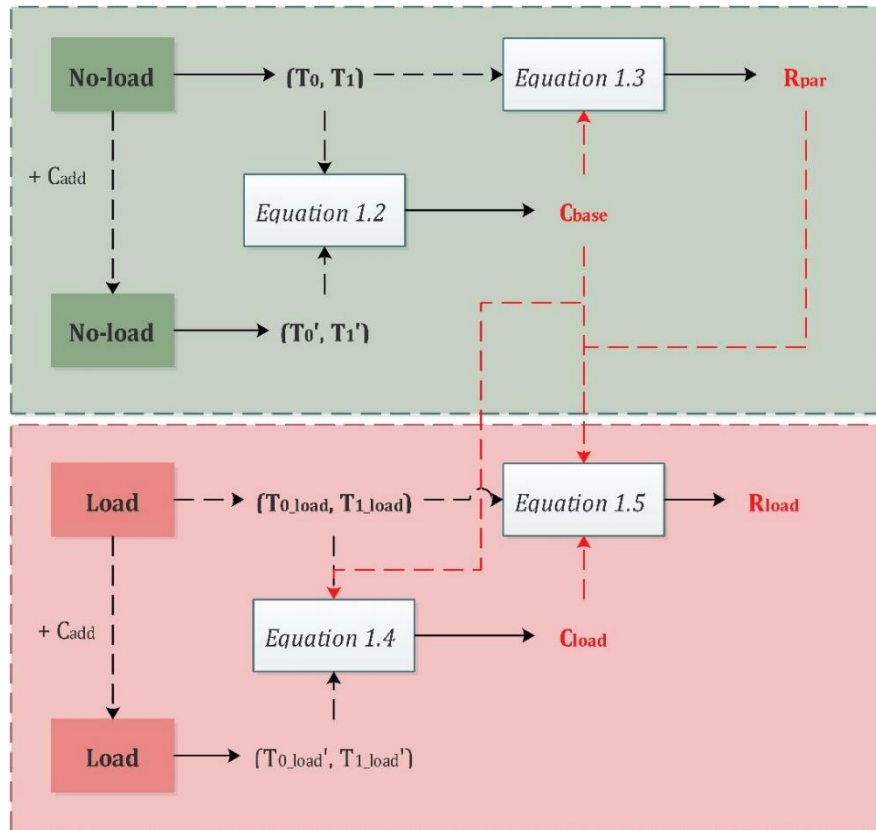


Figure 1.5. Calibration flow diagram for R and C calculation. (Diagram adapted from [6]).

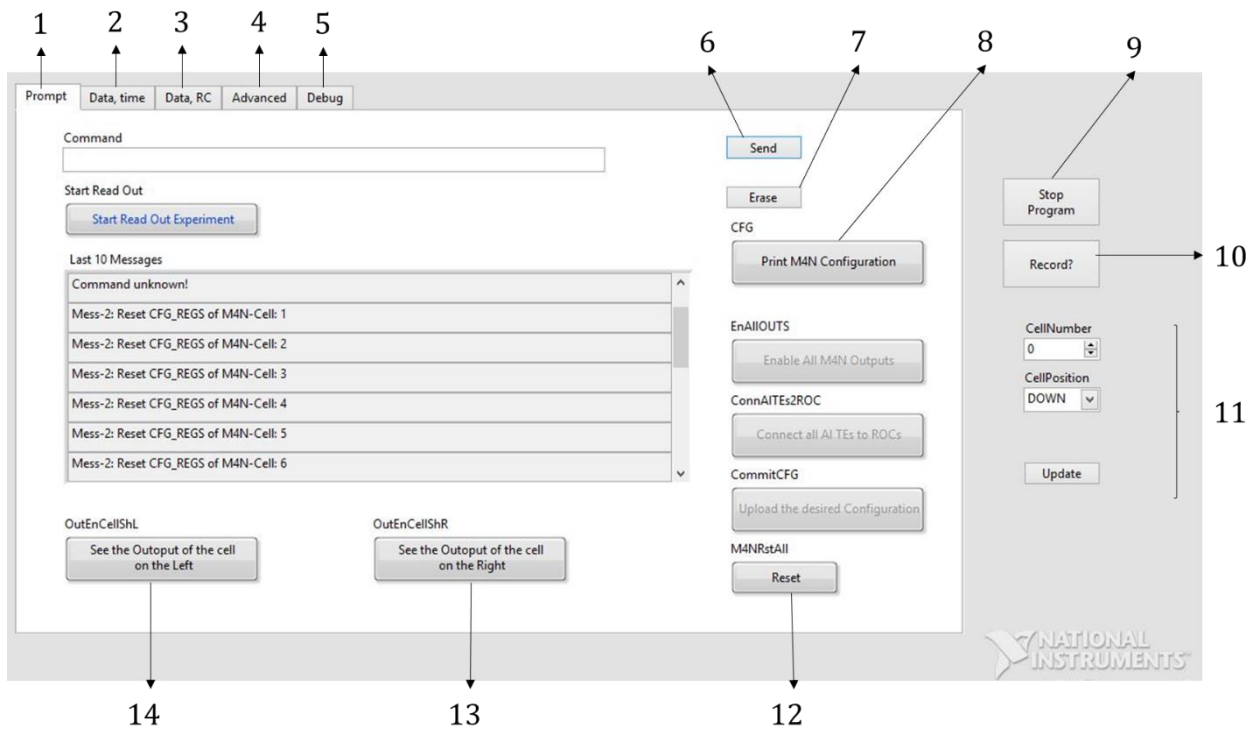
1.6 Electronic interface

A user-friendly Graphical User Interface (GUI) for the M4N system was developed by *Miccoli B.* in the National Instruments software LabVIEW. The interface allows to read and write data from the serial port and is formed by five constructive blocks or modules:

- i) Serial: communication with the serial port.
- ii) GUI: data visualization.
- iii) Event handler: detection of the commands defined by the user.
- iv) Recording: data saving.
- v) Control: all modules control system.

The software presents in a graphical way the serial input, in this case, values of T_0 and T_1 and the formulas explained in *Section 1.5.2* are implemented to give an instantaneous value of the correspondent R and C .

Figure 1.6 is a screenshot of the LabVIEW prompt page when the device is connected, and *Table 1.2* is a list of the most used serial commands.



1. Main window.
2. T_0 and T_1 visualization window.
3. R and C visualization window.
4. Advanced configuration window (calibration parameters and recording settings).
5. Debug control window.
6. Send button: sends the command written in the command space.
7. Erase button: erases what is written in the command space.
8. Print M4N configuration button: allows M4N current configuration visualization in the messages section (executes the command **PrintM4NCfg**).
9. Stop program button.
10. Record button: initializes the recording of the T_0 and T_1 values on a .txt file.
11. Controls for changing the cell displayed on the T_0 , T_1 , R and C graphs.
12. Reset button: resets all cells of the M4N (executes the command **M4NRstAll**).
13. See the output of the cell on the right button: changes the current M4N cell to the successive cell to the right (executes the command **OutEnCellShR**).
14. See the output of the cell on the left button: changes the current M4N cell to the preceding cell to the left (executes the command **OutEnCellShL**).

Figure 1.6 LabVIEW GUI main page screenshot.

M4N Main Serial Commands	
Command	Explanation
General Commands	
<i>PrintM4NCfg</i>	Prints the configuration of all the cells.
<i>CommitCFG</i>	Uploads the M4N configuration.
<i>M4NRstAll</i>	Reset all cells.
<i>M4NRstCell N</i>	Reset cell N (N=1,2,3,4,5,6,7,8).
<i>EnAllOUTS</i>	Enables all outputs of M4N.
<i>DiscAITes</i>	Disconnects all electrodes from CMOS circuits.
<i>OutEnCell N</i>	Changes the visible M4N cell output (N=1,2,3,4,5,6,7,8).
<i>OutEnCellShR</i>	Changes the visible M4N cell to the successive cell to the right.
<i>OutEnCellShL</i>	Changes the visible M4N cell to the preceding cell to the left.
<i>RunLoopExp N1 N2</i>	Runs loop experiments between cell N1 and N2.
<i>StopLoopExp</i>	Stops the loop experiment.
<i>SetNumMeasAvg n</i>	Sets the number of measurements for averaging.
<i>SingleMeas n</i>	Starts single measurement by using the M4N chip.
Calibration Commands	
<i>ROC2_optLeak N</i>	Optimizes of ROC2 leakage currents for M4Ncell N (N=3,4,6,7,8).
<i>ROC2_invPol N on/off</i>	Inverts ROC2 Polarity in cell N (N=3,4,6,7,8).
ROC2 Commands	
<i>ConnAITes2ROC</i>	Connects all the top electrodes to the ROCs.
<i>DefaultROCCfg</i>	Configures the M4N chip with the default ROC's values.
<i>EnROC2 N1 N2</i>	Enables ROC2 (only for cells 3,4,6,7,8) on electrode N2 (1,2,3).
<i>DisROC2 N1 N2</i>	Disables ROC2 (only for cells 3,4,6,7,8) on electrode N2 (1,2,3).
Dep Commands	
<i>ConnAITes2DEP</i>	Connects all top electrodes to DEP circuits.
<i>StopDEPAll</i>	Disables DEP on all M4N cells.
<i>DefaultDEPcfg N</i>	Set the DEP frequency to N (370k, 480k, 700k, 850k, 1M3, 1M8).
<i>SetDEPfreq N1 N2</i>	Sets the DEP for cell N1 to frequency N2.

Table 1.2. Main M4N serial commands.

2. Chapter II – Microelectrodes and Microchannels

Emerging technologies in the biosensing field have found several advantages on going to the *Micro* and the *Nano* scale such as production scalability, costs reduction, portability and simplicity for storage, reduction in the volumes and the analysis time, improved analytical performance and the possibility of multi-analyte platforms [2].

Scaling the electrode size to micro dimensions enhances sensitivity, selectivity, and mass transport phenomena at the surface. It also opens the possibility for the integration with microfluidic systems and therefore their application in cellular and molecular biology analysis [2].

Microfluidics attractiveness relies mainly on its ability to manipulate small amounts of fluids reducing drastically the volumes of samples and reagents needed to obtain sensitive and high-resolution outputs [2], [12].

Today the trend is to miniaturize and integrate electronics and fluidics in robust platforms able to perform analysis in self-contained miniaturized devices [2].

2.1 Overview on microfabrication technologies

By microfabrication technologies are understood the methods and techniques for “micro-products” manufacturing. According to *Luttge R.*, in its book *Nano and Microfabrication for industrial and Biomedical Applications: “Nanofabrication is a logical step to the further downscaling of the physical size of components and functional elements (...)”*[13].

Many kinds of materials are used in microfabrication: semiconductors, oxides, polymers and hybrid materials [13]. Main technologies (*Figure 2.1*) are briefly defined as follows dividing them into two categories: basic and advanced methods.

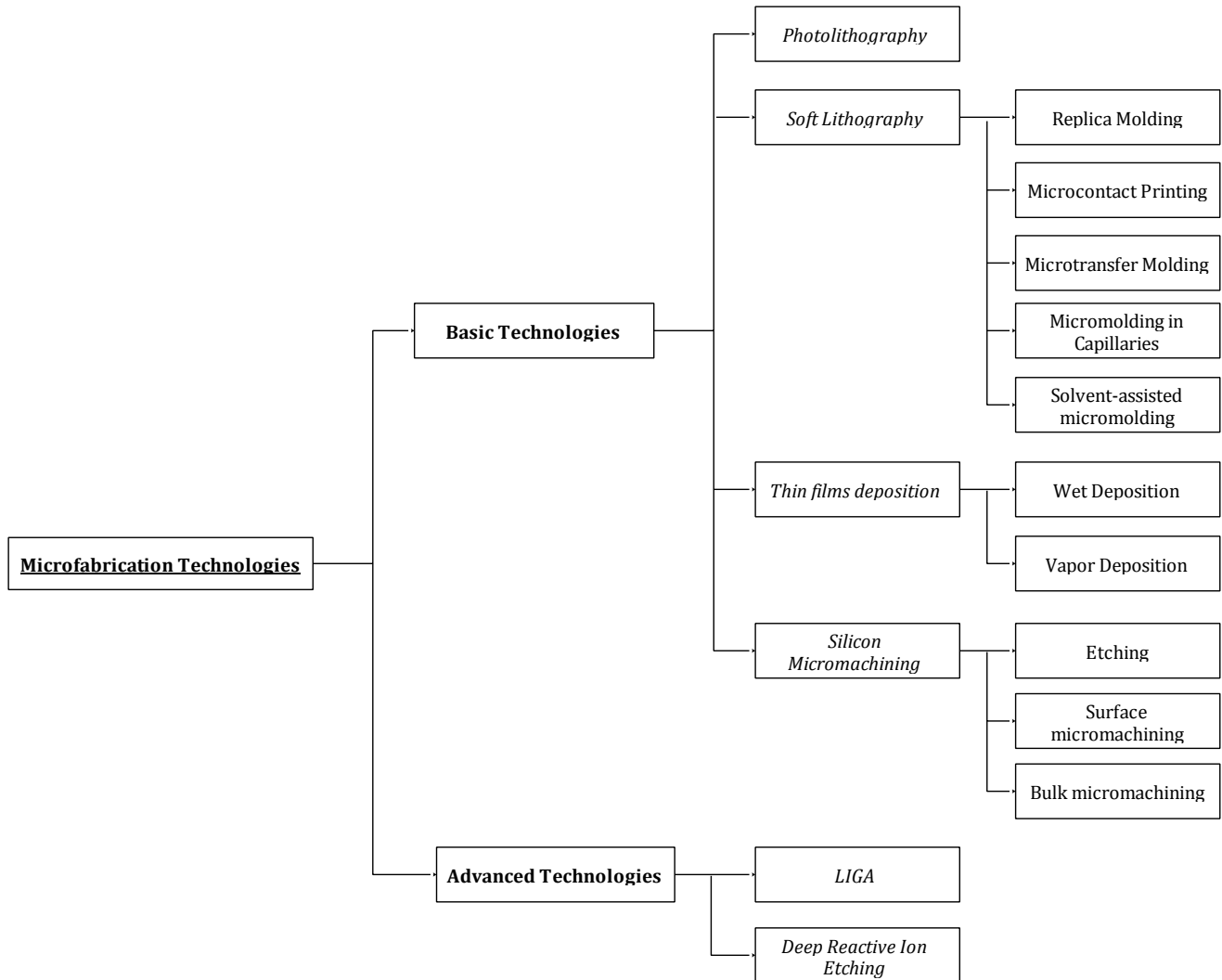


Figure 2.1. Microfabrication technologies (Scheme information from [13]).

2.1.1 Basic methods

i. *Photolithography*

Is a lithographic process that exploits the potential of photosensitive materials [13]. This technique is explained in detail in *Section 2.2*.

ii. *Soft-lithography*

It is a family of methods in which a patterned elastomer is used as a stamp. This stamp is usually obtained by casting from a master mold fabricated by lithographic techniques [14].

Soft-lithographic techniques include: replica molding, microcontact printing, microtransfer molding, among others [13].

iii. Wet and vapor deposition for thin films fabrication

In wet deposition processes the material is dissolved in a proper solvent and when spread onto the target substrate, the solvent evaporates letting the formation of a thin film.

Vapor deposition, on the other hand, is based on the sublimation of a material under vacuum conditions. When chemical synthesis takes place by adding precursors in the gas phase, the technique is called Chemical Vapor Deposition (CVD) [13].

iv. Silicon micromachining

Silicon, as the fundamental material of the semiconductor industry, is of great interest.

Silicon micromachining processes can be divided in three groups: etching, surface micromachining, and bulk micromachining. Etching consists on the removal of layers of material, two main modalities of the process are identified: wet chemical etching and dry etching. In wet etching, proper chemical agents react with the bulk material removing it in a controlled way. Dry etching, on the other hand, uses ions and a masking layer to selectively bombard the material [13].

2.1.2 Advanced methods

By advanced methods are understood the successive generation of microfabrication processes that opened the possibility to a wider range of materials and that combine electronics and other disciplines. Examples of this method are LIGA and Deep Reactive Ion Etching [13].

LIGA is the German acronym of Lithography (*Lithographie*), electrodeposition (*Galvanoformung*) and molding (*Abformtechnik*). In the process resist is developed with X-rays, then metal is deposited in the resist mold and after resist removal, a metal structure is obtained [15].

Deep Reactive Ion Etching (DRIE) is an etching technique that allows the fabrication of narrow and deep gaps. It derives from RIE (Reactive Ion Etching) that is a technique that combines physical (ions and plasma) and chemical mechanisms for etching. The main difference from classical RIE is the presence of passivation steps between etching steps [16].

2.2 Microfabrication by Photolithography

Lithography is a process that allows the replication of a pattern on a surface and it has been widely used for microelectronics and microfluidic applications. Optical lithography is a specific type of lithography that exploits light-sensitive polymers also known as “photoresists”. General steps of the process are:

1. *Substrate preparation or adhesion promotion*: the idea is to improve the adhesion of the photoresist to the substrate. There are three main processes that can be executed in this phase: cleaning of the substrate’s surface, water removal by dehydration and addition of adhesion promoters.
2. *Photoresist spin-coating*: allows the deposition of a thin and uniform layer of photoresist onto the substrate. It is first poured and then spun at high speed. Several parameters determine photoresist thickness and uniformity: type of deposition (static or dynamic), spin speed, resist volume, environmental temperature and humidity and inner properties of the resist and the substrate.
3. *Soft-bake or Pre-bake*: this process removes the solvent excess allowing the film to be stable at room temperature for later processes. Upon light exposure, photochemical reactions that change the solubility of the photoresist take place. Photoresists can be classified into two main groups according to their solubility in a solvent called developer. Positive photoresists are normally insoluble and become soluble by the exposure to light. Negative photoresists present exactly the contrary behavior. By means of a photomask, the resist is selectively exposed and it is possible to create patterns on the substrate. The way the photomask is used determines three types of processes: contact, proximity, and projection lithography.
4. *Post-exposure bake*: optional step driven by specific purposes such as components diffusion or additional chemical reactions.
5. *Development*: the resist is selectively removed following the exposition pattern.
6. *Hard-bake or post-bake*: optional step to harden the formed pattern by thermal stabilization.

7. Metrology and inspection: measurements for product and process control.
[17], [18].

The lithographic step is the starting point both for microelectrodes and microchannels for microfluidic systems fabrication as it provides as output the desired geometry.

For microelectrodes fabrication, the lithographic output is the negative of the desired geometry and the subsequent step is the metal deposition. Metal deposition can be achieved by sputtering. This process consists on the removal of atoms from a target material and their successive deposition on a substrate. The atoms are removed by the interaction with positive ions from plasma that are accelerated onto the target by an electric and/or a magnetic field. The process takes place under vacuum and most critical parameters are current and time [19], [20]. Sputtering is then followed by a lift-off process in which the metal that has been deposited on top of the resist is removed (as well as the resist), and the metal that has been deposited directly onto the substrate remains, obtaining the desired geometry.

For microchannels fabrication, the mask is usually fabricated by photolithography and the subsequent process depends on the material and the specific application. Typical materials include paper, glass, silicon, and polymer [12].

2.2.1 Output assessment: profilometry

An immediate measurement to assess the output of the lithographic process is the measurement of the surface profile. Profilometry allows the measurement of the dimensions of the obtained geometries. In microelectrodes fabrication, it allows measuring the thickness of the deposited metal that is a critical parameter.

Surface profile measurement techniques point towards a high resolution and a large dynamic range. There are several techniques for this purpose, and as shown in *Figure 2.2*, they can be classified into two major groups: optical and non-optical. Among the optical ones, optical interferometry-based techniques present advantages such as non-contact, high resolution and high precision [21].

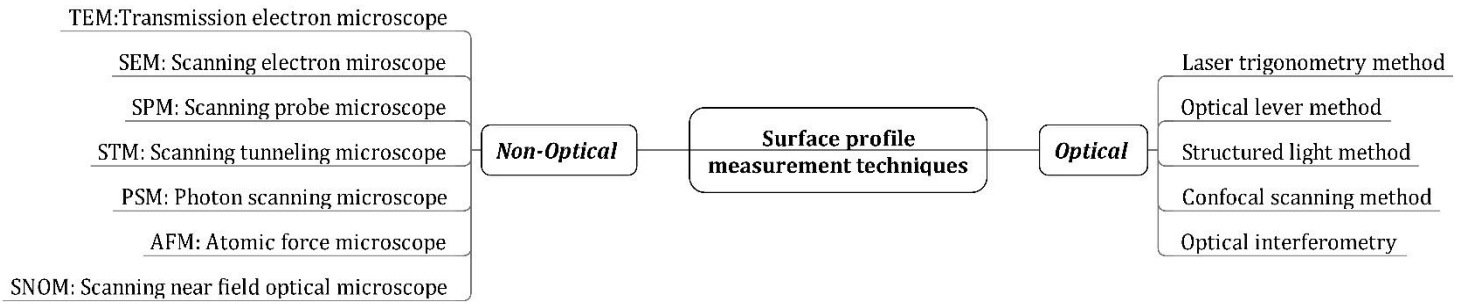


Figure 2.2. Surface profile measurement techniques summary scheme (Scheme information from [21]).

3. Chapter III –Cell impedance measurement

Impedance (Z) is defined as the complex ratio between voltage and current and has two parts: real (Z_{RE}) and imaginary (Z_{IM}). Magnitude and phase of impedance are presented in *Equations 3.1* and *3.2* respectively [22].

$$|Z| = \sqrt{(Z_{RE})^2 + (Z_{IM})^2} \quad \text{Equation 3.1}$$

$$\theta = \tan^{-1}\left(\frac{Z_{IM}}{Z_{RE}}\right) \quad \text{Equation 3.2}$$

Impedance analysis as explained by *Paez-Avilés. et al.*, is an electrochemical technique that gives information about changes in electrical resistance and capacitance at the surface of a substrate or electrode. This label-free and non-invasive technique has been proved to be useful for cell characterization in fluidic and microfluidic systems and for that reason is largely diffused in Lab-on-chip (LOC) devices [23].

3.1 Electric model of a single cell

The “Single-Shell” model is the typical and most simple model of a cell in which the cytoplasm is simplified as a sphere of a homogeneous phase surrounded by the plasma membrane modeled as a thin shell (*Figure 3.1.a*) [22].

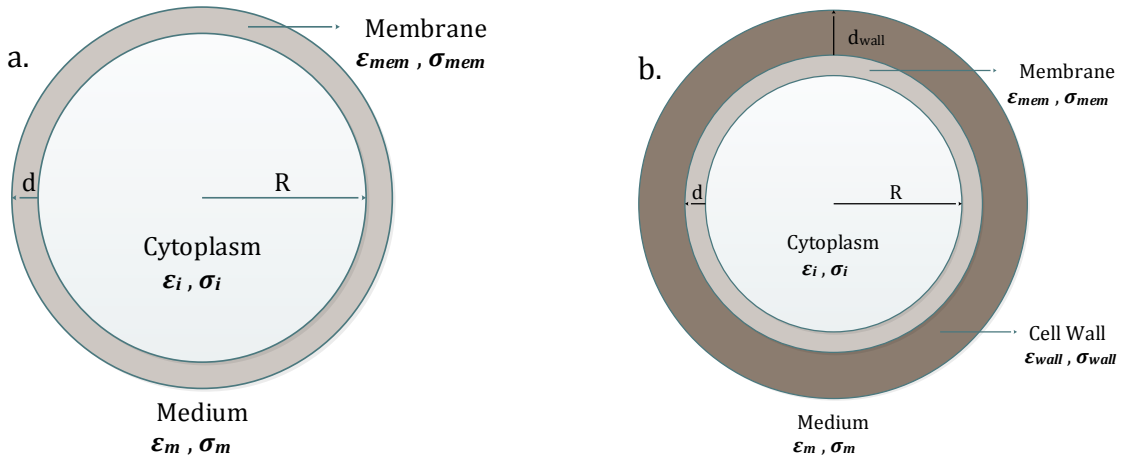


Figure 3.1. a) Single-Shell model. b) Double-Shell model (Image adapted from [22]).

In this model, factor ρ is defined as:

$$\rho = \frac{R}{R-d} \quad \text{Equation 3.3}$$

R: Cell radius.

d: Membrane thickness.

And the permittivity of the cell is:

$$\epsilon_{cell} = \epsilon_{mem} \left(\frac{\rho^3 + 2 \left(\frac{\epsilon_i - \epsilon_m}{\epsilon_i + 2\epsilon_m} \right)}{\rho^3 - \left(\frac{\epsilon_i - \epsilon_m}{\epsilon_i + 2\epsilon_m} \right)} \right) \quad \text{Equation 3.4}$$

ϵ_{cell} : Cell permittivity.

ϵ_m : Medium permittivity.

ϵ_{mem} : Membrane permittivity.

ϵ_i : Cytoplasm permittivity.

In the case of plant cells, bacteria and yeast that have a cell wall the electrical model becomes an analog “double-shell model” (Figure 3.1.b) [22].

A simplified electrical model of a single cell in suspension was proposed in 1989 by *Foster and Schwan*. The model consists of a resistor and a capacitor in series. The resistor stands for the cytoplasm and the capacitor for the membrane. The suspending medium is also represented by a resistor and a capacitor but this time in parallel. R and C components of the surrounding medium are at the same time in parallel to the cell R and C components (*Figure 3.2*) [24].

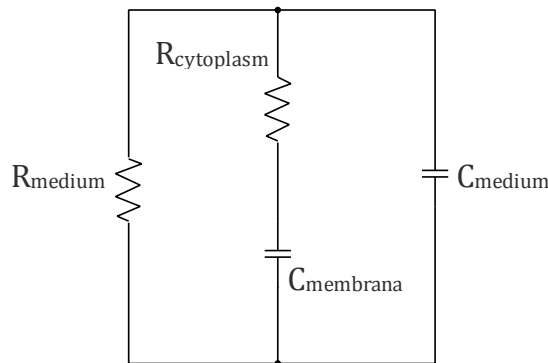


Figure 3.2. Electrical model of a single cell in suspension (Image adapted from [24]).

3.2 Cell impedance measurement techniques

Xu. et al., on their review report 3 different techniques for cell impedance measurement based on “The Single-Shell model” [22]:

- i. **Electric cell-substrate impedance measurement:** a technique for adherent cells. Cells adhered to electrodes can be analyzed as a Capacitance-Resistance equivalent circuit model, in which the optimal measurement region is between 100 Hz and 100 KHz.
- ii. **Impedance flow cytometry:** a technique for the measurement of cells through microfluidic channels. The geometry of both the channel and the electrodes play a key role. Optimal frequency range goes from 100 Hz to 10 MHz.
- iii. **Impedance spectroscopy of cells in suspension:** usually used for detection or proliferation monitoring [22].

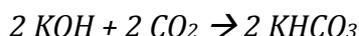
Cells impedance spectrum can be divided in various regions. At very low frequencies, current cannot pass the cell membrane and impedance and, with a proper set-up, impedance can give an idea of the cell size. Such is the case of the Coulter Counter that will be explained in *Section 3.3* [25]. Low frequencies impedance changes correspond also to the double layer capacitance and the resistance of the charge transfer at the suspension-electrode interface [26]. At intermediate frequencies, impedance gives information about the cell membrane as membrane polarization phenomenon is reduced. Higher frequencies intracellular organelles and cell cytoplasm dominate as the cell membrane is minimally polarized [22], [25], [26].

3.2.1 Yeast cells and impedance measurement

Yeast (*Saccharomyces cerevisiae*) as a laboratory cell eukaryotic model presents two main advantages: easy to manipulate and fast growth rate. Yeasts are surrounded by a cell wall made of glycosylated glycoproteins, β -glucans and chitin. Components proportions are highly dependent on growing conditions. Like other eukaryotic cells, yeasts have a cytoskeleton, a periplasmic space and a plasma membrane [27].

Yeasts appear also interesting for laboratory studies as they are involved in industrial fermentation processes such as wine, beer and bread production [28].

A technique found in literature for yeast vitality analysis is the indirect impedance measurements. In this technique yeast are monitored by means of the CO_2 production as an indicator of their metabolism and therefore of their vitality. The technique contemplates the addition of a 0.2% KOH solution to the culture medium. The KOH absorbs the CO_2 produced by the yeast's metabolism and causes a decrease on the impedance [29]–[31]. The chemical reaction is [29]:



Equation 3.5

Impedance measurement as a vitality test could be used as an indicator for fermentation capability when the variable measured is the time taken to reach a certain impedance change value. This parameter is usually known as “detection time” and provides information about the lag phase duration [30].

For yeasts culture monitoring, *Posseckardt et al.* found that in the low frequency region, from 0,01 Hz to 10 kHz, impedance was dominated by the double-layer capacitance, while from 10 kHz to 1 MHz, impedance was dominated by the resistance of the solution at the electrode interface [26].

3.3 Microfluidic Chips for cell impedance measurement

Impedance measurement as a label-free technique presents several advantages such as cost reduction, since it does not need immunological markers, sample preparation time reduction compared to fluorescence analysis and what is perhaps most interesting for bio-applications, the ability to measure without perturbing the system. These characteristics make it suitable for its use in integrated platforms [25].

Microfluidic chips, attractive because of the low size and cost, compared to conventional instruments, have a great number of potential applications in cell analysis. Measuring dielectric properties of cells can give information about the cell membrane or the cytoplasm that can be correlated with physiological or pathological changes. Other applications of this kind of measurements include particle counting, cytometry and cell viability. Specifically, multifrequency measurements have been proved to provide high-content data that can be used for cell type discrimination and drug screening [25].

One of the most spread and studied applications of microfluidic chips is the so-called “microfluidic impedance cytometry” that is a miniaturized variant of the Coulter Counter. The Coulter Counter, that takes its name from its developer, is a device that measures DC resistance. It consists of two chambers connected by a small channel. The chambers are filled with a conductive fluid and two electrodes are placed at each side of the channel. When a particle passes through the channel changes the resistance measured as a current pulse. Each pulse corresponds to a particle. In other words, the Coulter Counter is an impedance cytometry system based on current modulation [24].

Typical fabrication techniques for microfluidic chips are micromachining techniques and molding. Among molding techniques, the most spread one is soft lithography [25].

4. Chapter IV – M4N Experimental part

4.1 M4N Chip assembly

- Objective: assembly functional M4N chips for their use in subsequent measurement experiments.

4.1.1 Experimental design: material and methods

Materials:

- M4N chip.
- M4N adapting board.
- Thin wires for bonding.
- Resin.
- Welding equipment.

M4N are assembled following the procedure shown in the flux diagram of *Figure 4.1*.

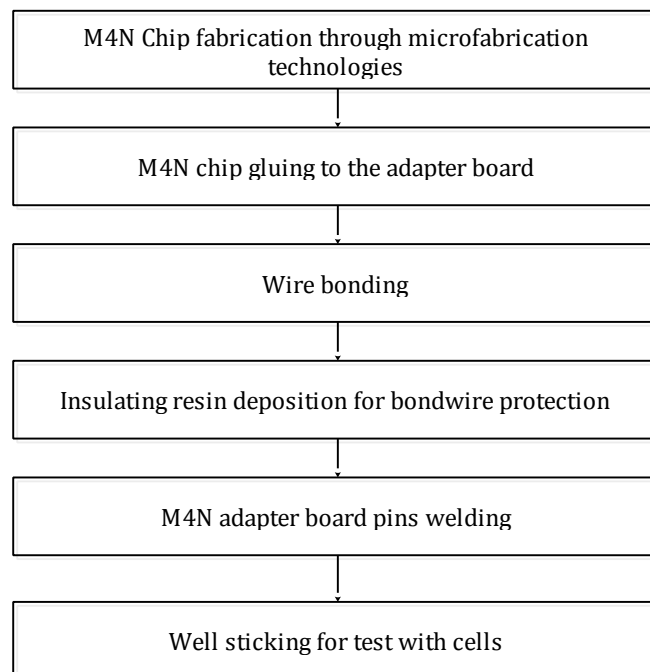


Figure 4.1. Flux diagram of the M4N assembly process.

4.1.2 Results and discussion

M4N chips were assembled following this methodology. Once the M4N is assembled and pins are welded, a quick test through the “Serial Monitor” of Arduino is performed to check that the circuits are working (DEP⁴ and ROCs⁵ circuits).

The main result of this process is a ready to use M4N for measuring (*Figure 4.2*).

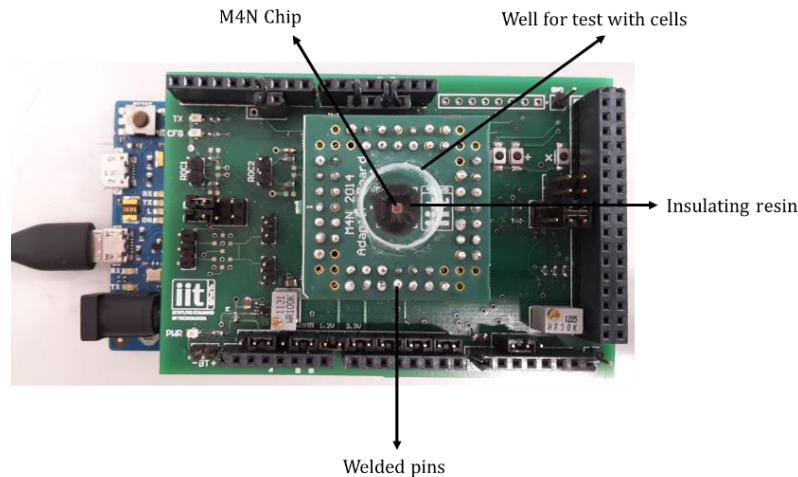


Figure 4.2. Assembled M4N ready for testing.

Once assembled initial characterization consisted of optical microscopy of the M4N. *Figure 4.3 (a)* is an optical microscopy image that shows the 8 SoC. *(b)* and *(c)* correspond to further optical magnification and the three typologies of electrodes can be identified.

⁴ DEP: Dielectrophoresis.

⁵ ROCs: Read-out circuits.

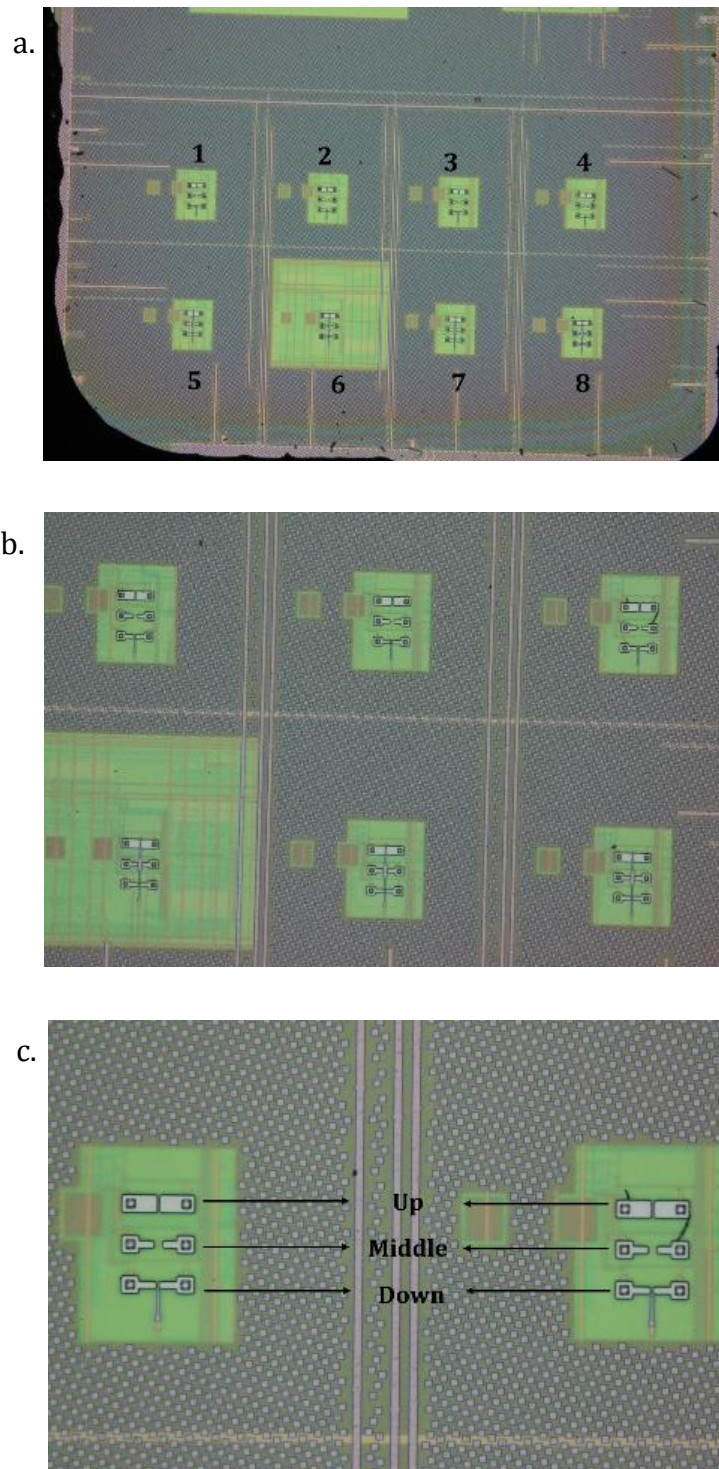


Figure 4.3. Optical microscopy of M4N a) Eight SoC (5x) with the standard cell numeration. b) 10x
c) Two M4N cells in which up, middle and down electrodes are identified (20x).

4.2 M4N calibration

- Objective: the main scope of calibration procedure, as described by *Bonanno. A*, is to estimate the non-idealities of the Read-Out-Circuit [9].

Calibration was executed just for a single chip because, as will be explained in *Section 4.3*, later experiments were carried in terms of T_0 and T_1 .

4.2.1 Experimental design: material and methods

Materials:

- M4N Chip, interface board and Arduino Due.
- Resistors and capacitors (5% tolerance).
- Multimeter.
- Oscilloscope.

The calibration procedure was followed as explained in *Section 1.4.2* for R and C calculation.

For calibration, middle aluminum top electrodes ($AlTE_{mid}$) of cell number 6 were used as they are connected both to the ROC and to the pads. The procedure foresees the use of external resistors and capacitors that simulate the measured values of R and C. Components were chosen with a 5% tolerance and the “*two-step algorithm for circuit calibration*”, proposed by *Bonanno. A*, was followed [6]. The calibration procedure is recapitulated in the flux diagram in *Figure 4.4*.

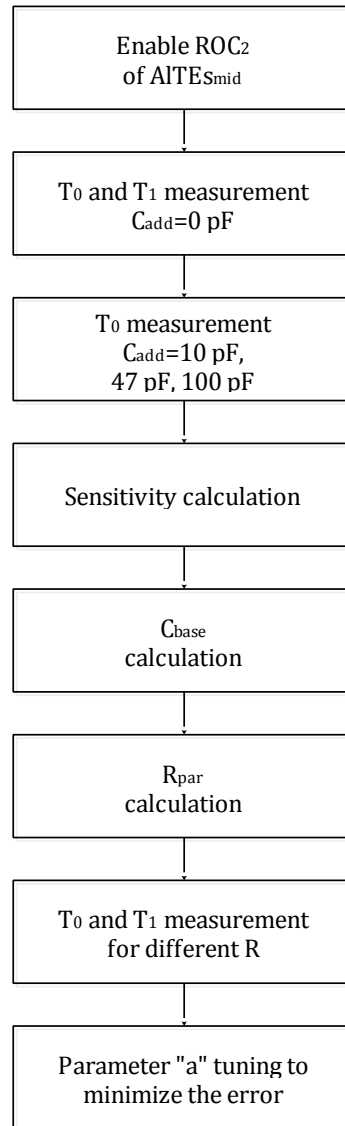


Figure 4.4. Flux diagram of the executed calibration process.

4.2.2 Results and discussion

Main Calibration steps with their results:

1. Enable ROC_2 of $ALTES_{mid}$.
2. T_0 and T_1 measurement with $\Delta C = C_{add} = 0$ pF (Table 4.1).
3. T_0 measurement with $\Delta C = C_{add} = 10$ pF, 47 pF, 100 pF. Reported T_0 and T_1 correspond to a mean value of 100 samples. (Table 4.1).

	Cadd (pF)	T0 (μ s)	T1 (μ s)
C1	0	1,2032	208,5790
C2	10	1,6639	-
C3	47	3,2125	-
C4	100	5,3044	-

Table 4.1. T_0 and T_1 for $C_{add} = 0$ pF. T_0 values for different C_{add} .

4. With $\Delta T=(T_0'-T_0)$ and $\Delta C=C_{add}$, ROC's sensitivity is calculated (Table 4.2).

No load		
C' (pF)	C'' (pF)	$\Delta C/\Delta T_0$ (pF/ μ s)
0	10	21,7053
0	47	23,3912
0	100	24,3829

Table 4.2. Sensitivity calculation.

5. C_{base} calculation (Equation 1.5).
 6. R_{par} calculation (Equation 1.6).

$\Delta C/\Delta T_0_{avg}$	23,1598
C_{base}	27,8651
R_{par}	89,8238

Table 4.3. Mean sensitivity, C_{base} and R_{par}

7. Measurement of a couple of resistors within the range allows to choose the constant "a" between a range from 4 to 12 in order to minimize the error. Systematic error due to the assumed approximations for R and C calculation is defined by Equation 4.1 [11].

$$Error (\%) = \frac{|R_{measured}-R_{nominal}|}{R_{nominal}} \quad \text{Equation 4.1}$$

Nominal resistance of the tested resistors was obtained by simple multimeter measurement. As can be seen in Table 4.4, for commercial resistors $R=15 \text{ M}\Omega$, $20 \text{ M}\Omega$ and $24 \text{ M}\Omega$, the error is minimized when $a=12$.

T0 (μ s)	T1 (μ s)	C (pF)	R (M Ω)	C_calc (pF)	R_calc (M Ω)	Errore (%)
1,300	34,863	0	16,8	2,2426	16,43821012	2,1535
1,296	39,895	0	19,8	2,1500	19,39370682	2,0520
1,285	45,508	0	23,5	1,8952	23,0608036	1,8689

Table 4.4. Obtained R and C for 3 different simulated R values and the systematic error, with $a=12$ and assuming the simulated C as zero.

Calibration parameters are summarized in *Table 4.5*.

Calibration Parameters	
a	12
C _{pad}	13
C _{int}	14,8651
Delta_C/Delta_T	23,1598
C _{base}	27,8651
T0 _{no load}	1,2032
T1 _{no load}	208,5790
R _{par}	89,8238

Table 4.5. Calibration parameters.

4.3 M4N characterization in aqueous environment

A first experiment consisted on an analysis of the M4N behavior with different solutions. Analysis was carried in terms of T₀ in T₁ because measuring with the M4N electrodes in absence of nanowires or any other sensing nanomaterial is very likely to go out of the R and C measuring range.

Main objectives of this characterization are:

- i. Identify if the M4N is suitable for measurements in aqueous environment from both physical and functional point of view.
- ii. Analyze T₀ and T₁ trend upon comparison between different cells of the M4N.
- iii. Compare trend and measurements of couple of electrodes with different gap (up, middle, down) in order to recognize the influence of this parameter.

All the measurements were repeated with a M4N Chip in which gold nanoclusters were deposited through a gold sputtering process. The scope of this was to understand how the presence of gold nanoclusters affected the measurements.

A second experiment consisted on the impedance measurement of the same solutions with interdigitated gold electrodes and an impedance-meter in order to study the impedance response and behavior of the different solutions. This last part was done with the purpose to understand if any relation could be inferred from the data obtain with the M4N.

4.3.1 Experimental design: material and methods

Materials:

- M4N Chip, interface board and Arduino Due.
- Interdigitated gold electrodes.
- Distilled water and tap water.
- Yeast cells in culture medium: yeast cells were suspended in the commercial Oxoid Signal® Blood Culture System that is a medium composition that enhances the growth of aerobic, anaerobic and microaerophilic organisms. It is intended for the detection of micro-organisms in blood samples. It has a 7.0 pH [32].

Equipment:

- Microscope.
- Impedance-meter: Keysight Technologies E4990A impedance analyzer.

A first experiment consisted on the deposition of a single drop (3,5 μl) of 4 different solutions: distilled water, tap water, blood culture medium and yeast cells in blood culture medium.

T_0 and T_1 were acquired by the LabVIEW software. Since T_0 and T_1 reached stability in a few minutes, measures were performed for short time intervals (around 3 minutes). For mean calculation and analysis, 300 data points were considered.

The M4N cells used for this experiment were cells 3, 4, 7 and 8. For each cell, “Up”, “Middle” and “Down” electrodes were considered with each one of the 4 solutions, giving therefore 48 measurements. Cells 1, 2 and 5 were not considered because they have a different typology of Read-Out-Circuit. Cell 6 was not considered in this experiment because as it is also connected to the PAD and its output is affected by an additional parasitic resistance and basal capacitance that directly affects T_0 and T_1 .

Measurements were repeated with a M4N in which gold nanoclusters were deposited by sputtering. Sputtering process was done with a current of 20 mA for 20 seconds. Down couple of electrodes of cell number 4 was selected for comparison ($AlTE_{\text{down}}$).

In order to understand better the impedance behavior of the studied substances, a second measurement set was done with interdigitated electrodes. The experimental set-up is presented in *Figure 4.5*. In this experiment, a volume of 100 μl was disposed on the well. The studied frequency range goes from 20 Hz to 1 MHz. Further information and technical specifications about these electrodes will be presented in *Section 5.3*.



Figure 4.5. Impedance measurement in well.

4.3.2 Results and discussion

In Figure 4.6, mean values of T_0 and T_1 of all the 48 measurements are presented to have a global idea of the data set. Variation of both parameters in comparison with T_0 and T_1 values in absence of any substance (air) is smaller in the case of distilled water and tap water, while blood culture medium and yeast cells exhibit greater variation. It can also be noticed that blood culture medium and yeast occupy a greater area in the T_0 - T_1 plane implying a greater variation between measurements. This phenomenon is attributed to the fact that both blood culture medium and yeast cells are more dynamic systems, but also to outlier measurements that will be explained ahead.

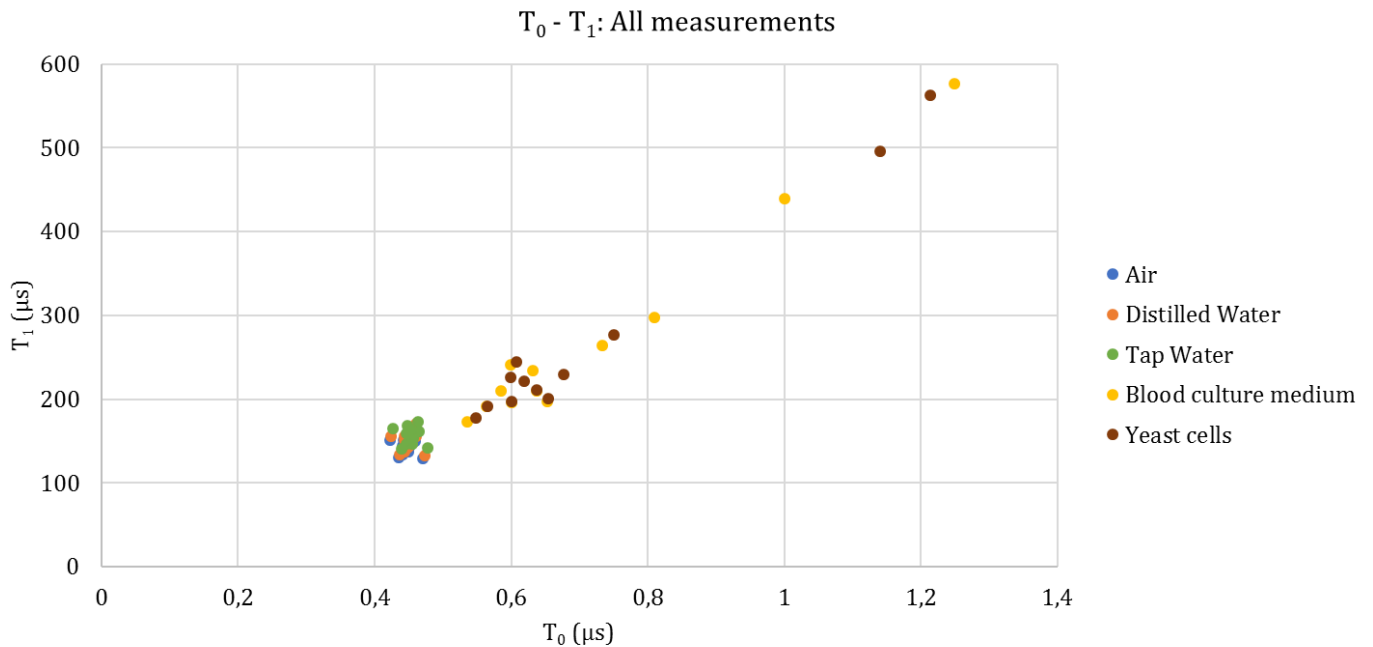


Figure 4.6. T_0 - T_1 Plane with all the measurements.

On the box and whiskers plots of the data set represented in *Figure 4.7*, the outlier data on medium and yeast measurements is made evident. Blood culture medium shows the greater variability.

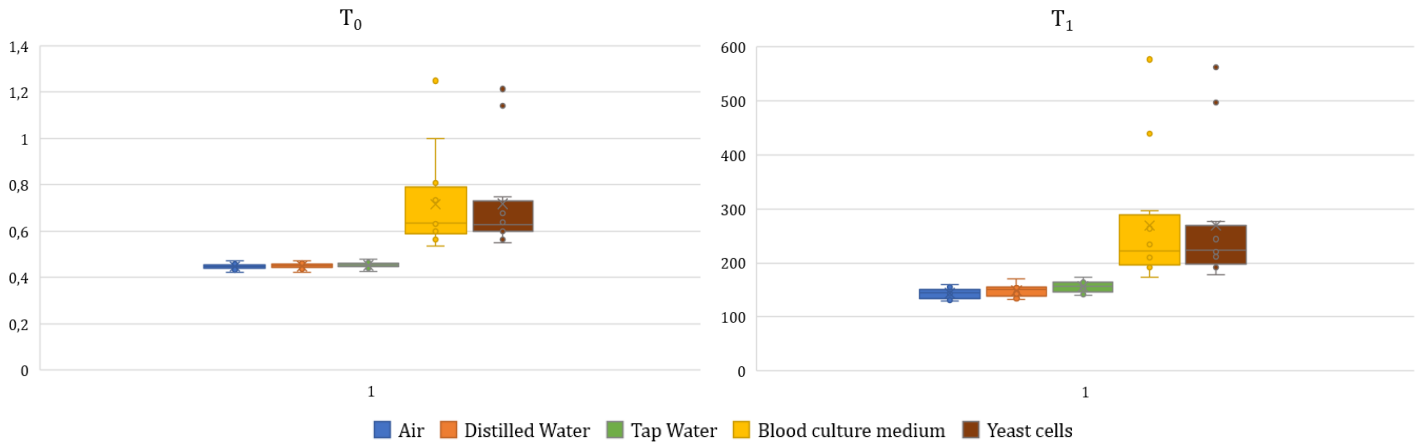


Figure 4.7. T_0 and T_1 Box and Whiskers plots for all the measurements.

Focusing on yeast and blood culture medium, from *Figure 4.8* it can be observed that while measurements for “Up” and “Down” cells are very similar, “Middle” measurements differ significantly. Specifically, middle electrodes of cells 3 and 8 are the most distant values. When observing these two cells at the microscope, oxidation was observed upon one of the middle electrodes, causing, with a high probability, this somehow “outlier” data (*Figure 4.9*).

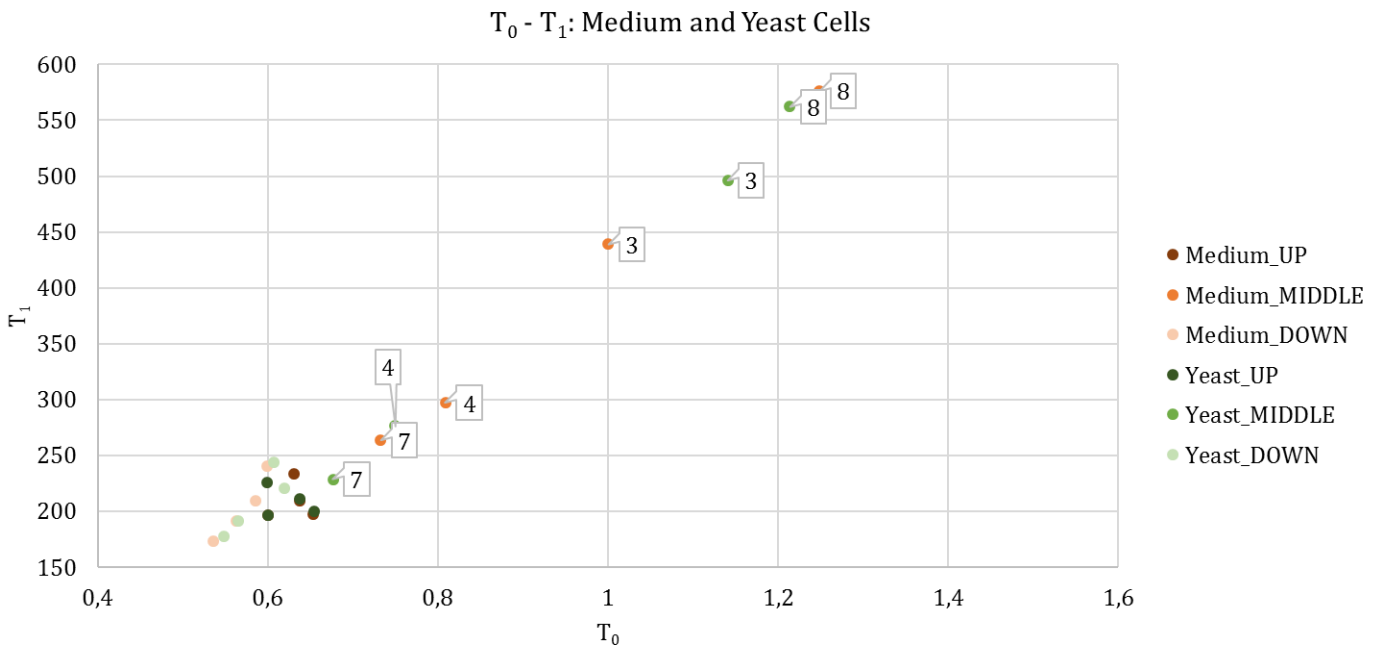


Figure 4.8. T_0 - T_1 Plane with measurements for blood culture medium and yeast cells.

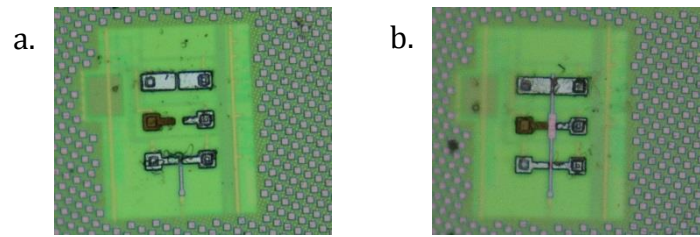


Figure 4.9. Microscopy images of a) cell 3 and b) cell 8. In both cases oxidation is observed in one of the middle electrodes.

Focusing furthermore on “Up” and “Down” couples of electrodes, T_0 and T_1 were normalized to air measurement in order to obtain a relative variation of both parameters. Average values are presented in Figure 4.10.

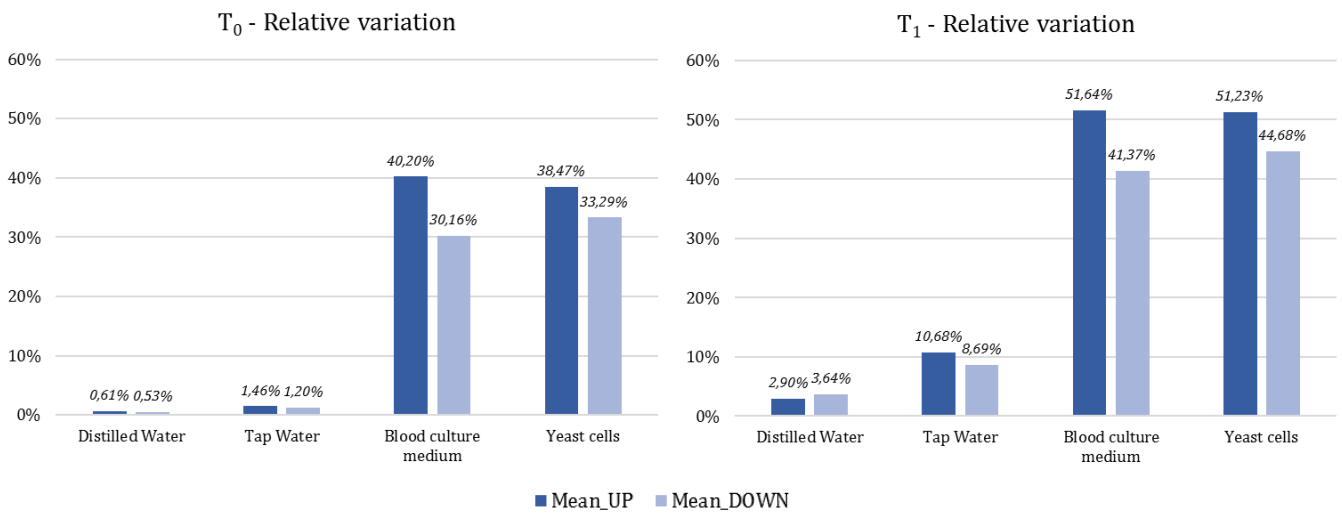


Figure 4.10. T_0 and T_1 relative variation of cells “Up” and “Down”.

From Figure 4.10 a greater relative variation of “Up” couples of electrodes is observed. Highest variation between these two typologies of electrodes is found for blood culture medium (around 10% higher than yeast cells for both T_0 and T_1). From these results, relation between gap distance and sensibility, for this particular kind of measurement can be inferred. Further studies are suggested to confirm it.

In Figure 4.11 and Figure 4.12, T_0 and T_1 graphs of a single cell are presented to illustrate the T_0 and T_1 trend with the different substances. Values presented correspond to $AlTE_{down}^6$ of cell number 4, for 300 samples.

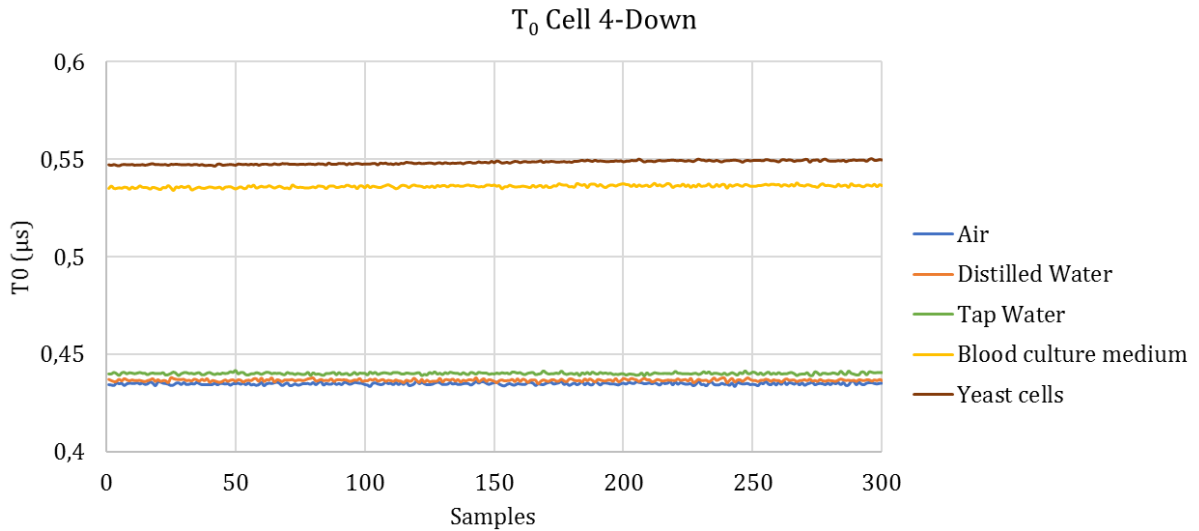


Figure 4.11. T_0 values for $AlTE_{down}$ of cell 4 for 300 samples.

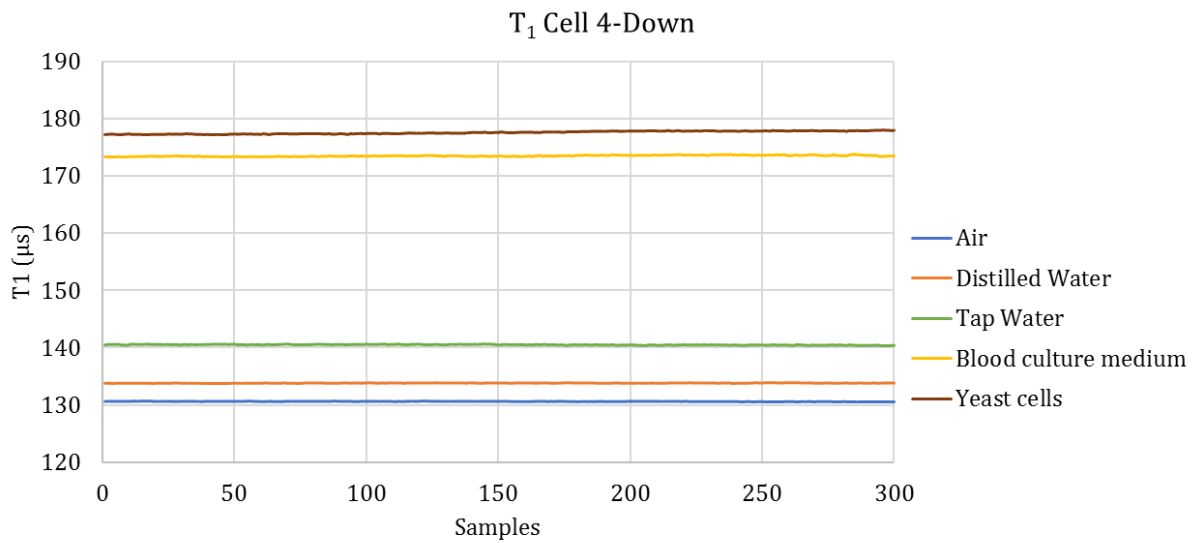


Figure 4.12. T_1 values for $AlTE_{down}$ of cell 4 for 300 samples.

As the trend was consistently observed in all the couples of electrodes, the results are presented in radar charts. These charts, intended to present in a graphical way multivariate data gives a quick idea of the symmetry of the obtained values. Graphs are presented for T_0 and T_1 of each typology of electrodes (Up, Middle, Down).

⁶ $AlTE_{down}$: Down aluminium top electrode.

T_0 and T_1 measurements for “Up” couples of electrodes (gap distance: 2,5 μm) are presented in *Figure 4.13*.

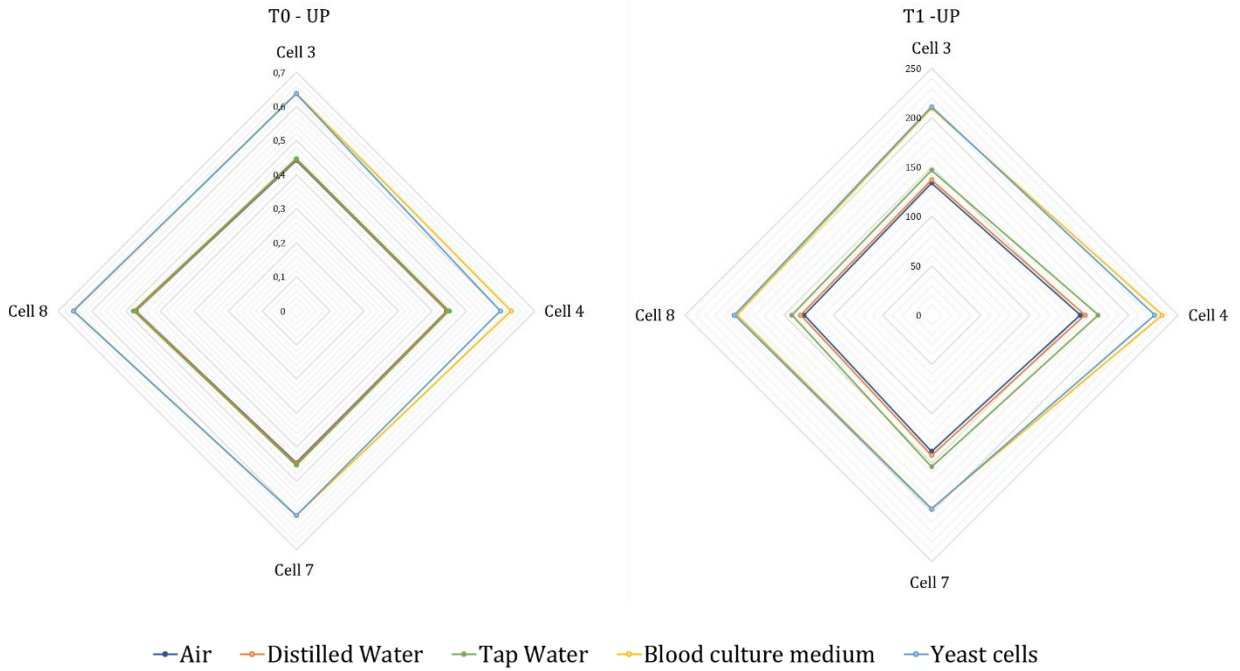


Figure 4.13. T_0 and T_1 for “Up” couple of electrodes.

T_0 and T_1 measurements for “Middle” couples of electrodes (gap distance: 10 μm) are presented in *Figure 4.14*. A great variation is observed on cells 3 and 8, attributed, as mentioned before to corrosion phenomenon observed in this two couples of electrodes (*Figure 4.9*).

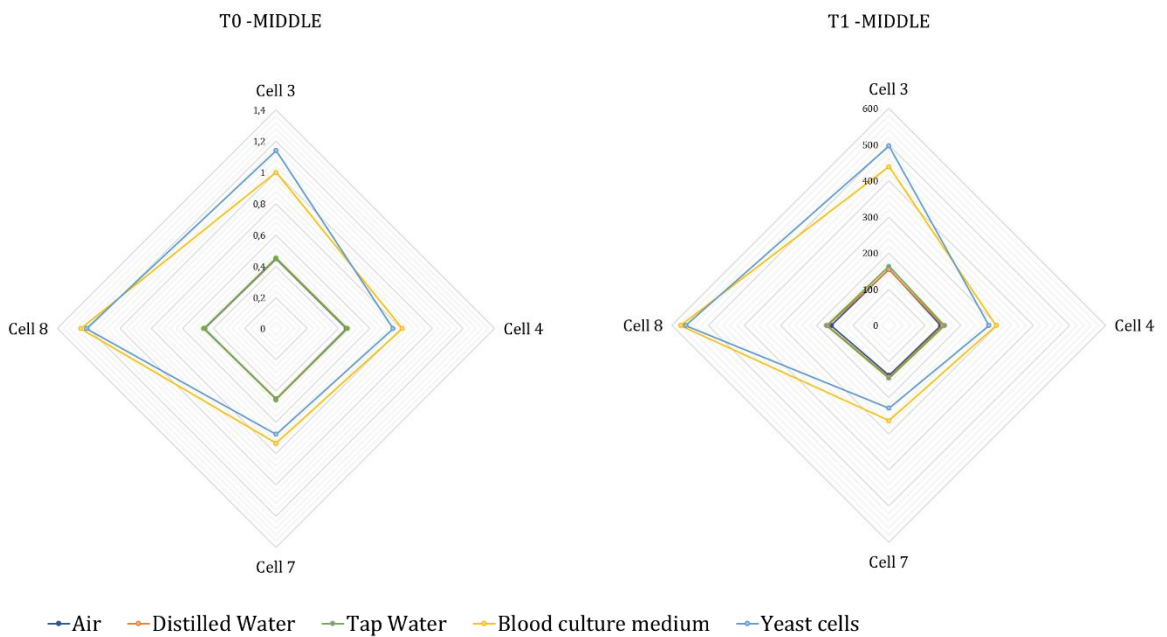


Figure 4.14. T_0 and T_1 for “Middle” couple of electrodes.

T_0 and T_1 measurements for “Down” couples of electrodes (gap distance: 7,5 μm) are presented in *Figure 4.15*.

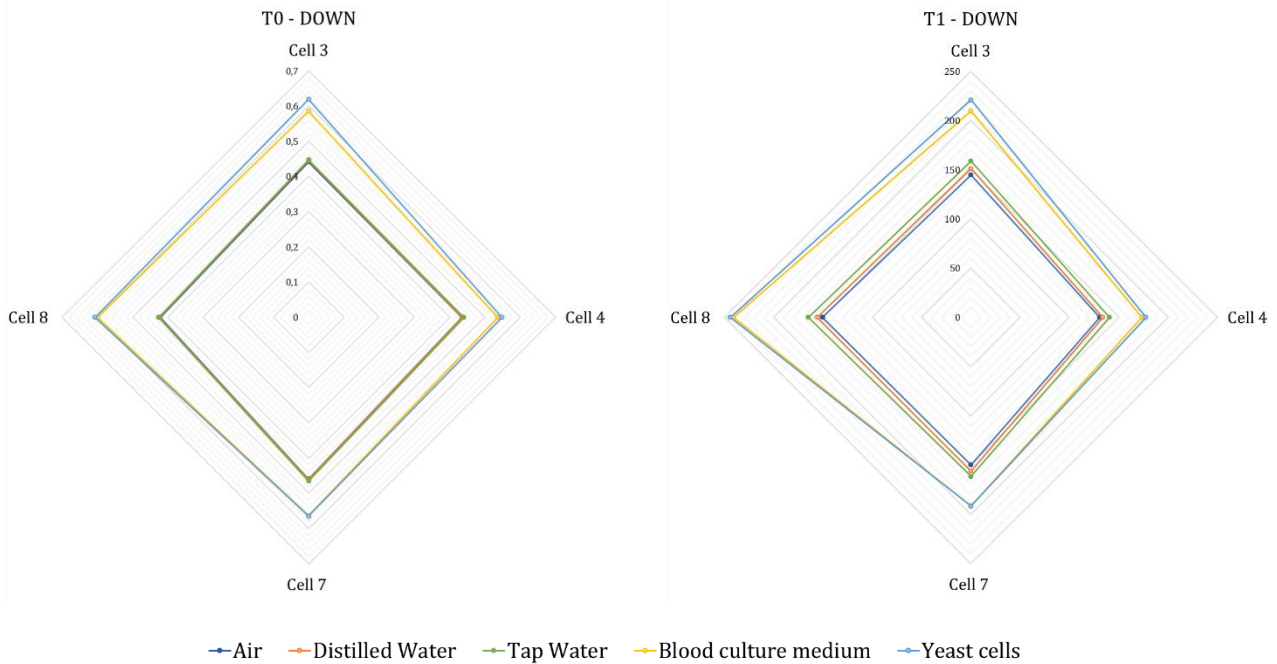


Figure 4.15. T_0 and T_1 for “Down” couple of electrodes.

As can be easily observed in the radar charts, for all the measurements T_0 and T_1 show the same global behavior. Measure is shown to be affected by bubbles formation and corrosion of the electrodes.

For better measurements comparison with gold nanoclusters, relative change on T_0 and T_1 parameters were calculated as the percentage change respect the air measurements. Variation of both parameters with and without gold nanoclusters for “Down” couple of electrodes of cell number 4 are presented in *Figure 4.16*.

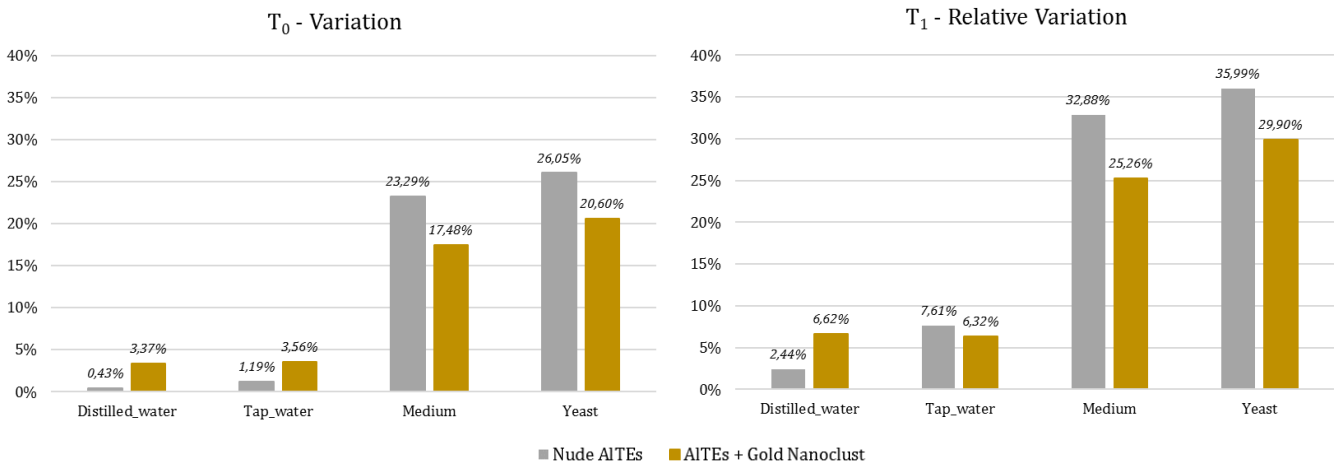


Figure 4.16. Relative variation of T_0 and T_1 with and without gold nanoclusters.

Percentages with gold nanoclusters for medium and yeast cells are lower than percentages of nude aluminum electrodes. No advantages are observed from the gold sputtering process.

The second experiment made with interdigitated gold electrodes gave the impedance response presented in *Figure 4.17*. Impedance was measured in the frequency range from 20 Hz to 1 MHz and the acquired impedance ranged from around 50 Ω to around 12 k Ω .

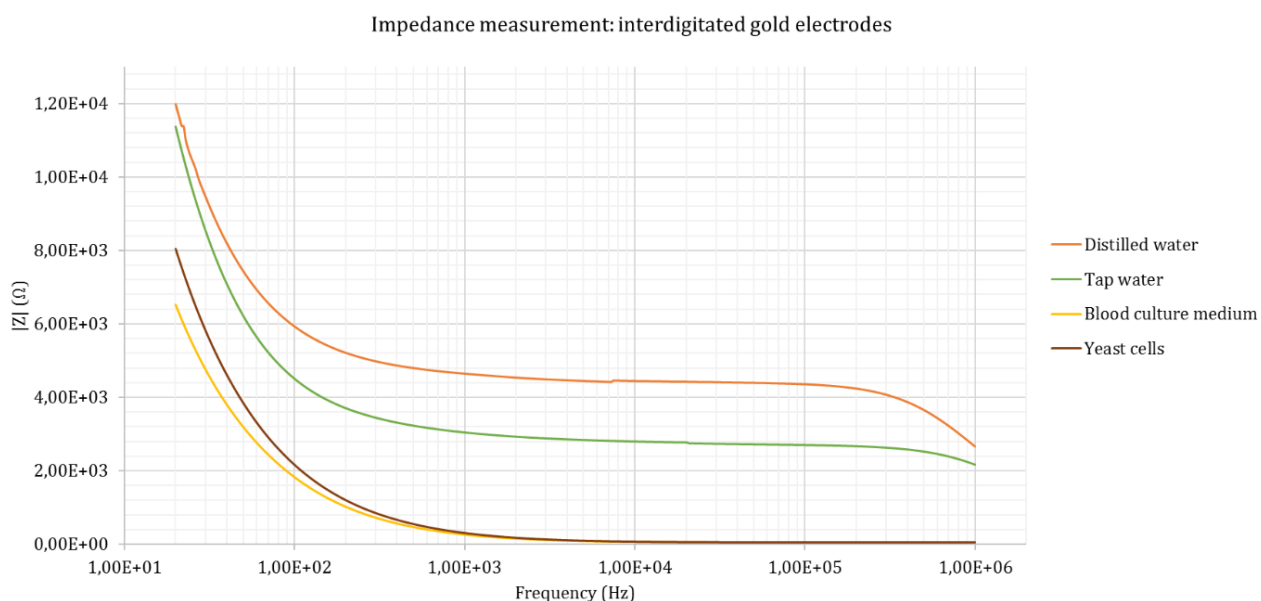


Figure 4.17. Impedance measurement curves for the 4 solutions (frequency axis in logarithmic scale).

Further analysis was done in a frequency interval that presents a relative stable measurement. This is reported in literature to be of interest for cell substrate impedance measurement: 100 Hz- 100 kHz [22]. Mean, minimum and maximum values within this frequency range are summarized in *Figure 4.18*. Yeast cells show the greater variation range in the analyzed frequency interval.

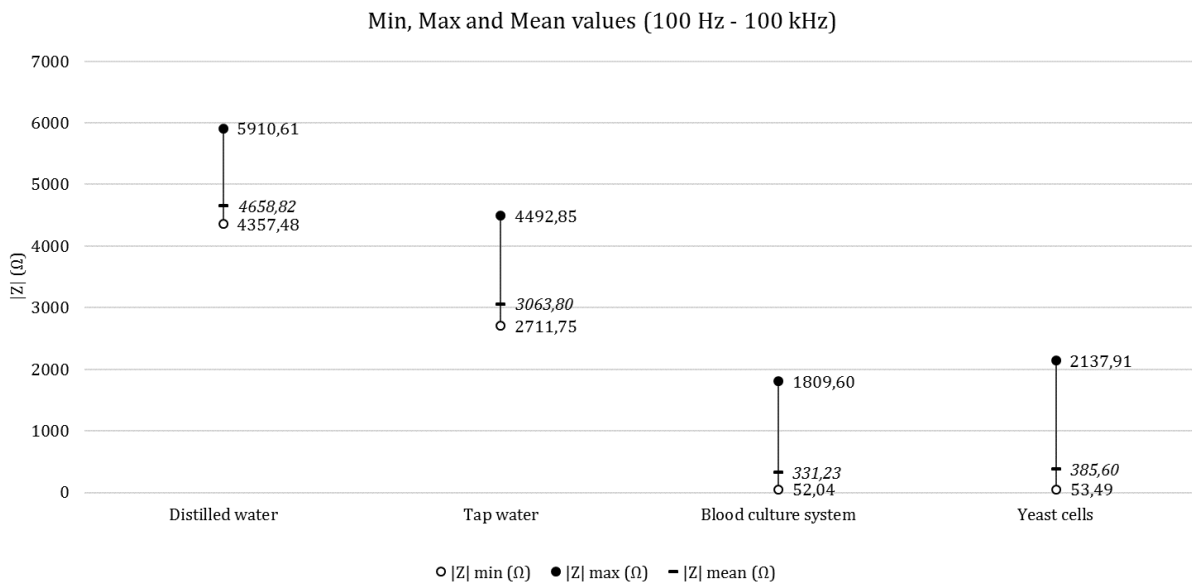


Figure 4.18. Impedance measurements of interdigitated gold electrodes in the range [100 Hz - 100 kHz]

To further understand the difference between blood culture system with and without yeast cells, impedance curves for both systems are presented in Figure 4.19. It can be concluded that the presence of yeasts causes an increase in the impedance value.

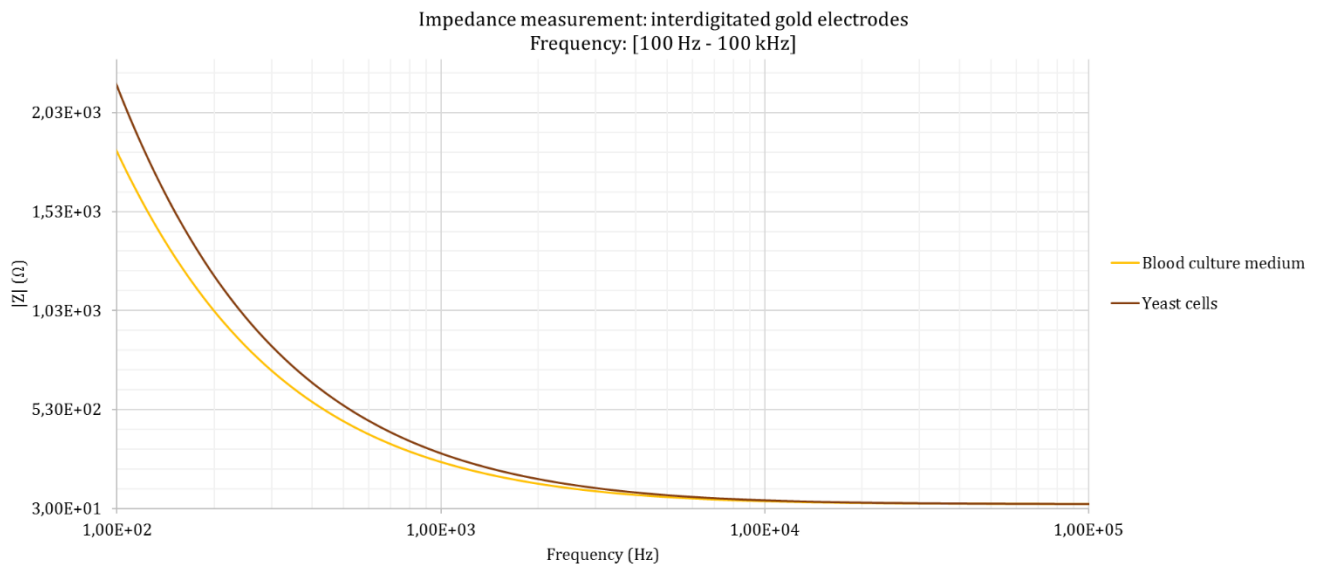


Figure 4.19. Impedance measurement curves for blood culture medium with and without yeast cells in the frequency range from 100 Hz to 100 kHz (frequency axis in logarithmic scale).

Further experiments, specifically quantitative analysis, are needed in order to determine if the platform is suitable for cell sensing applications, and further optimization of process parameters is needed.

An experiment in which optical microscopy is executed contemporary to electrical measurements is strongly suggested.

5 Chapter V – Microelectrodes and Microchannels Experimental part

5.1 Microelectrodes fabrication

- Objective: fabrication of gold microelectrodes with two different geometries: interdigitated and trident-shape.

5.1.1 Experimental design: material and methods

Materials:

- Substrate: Si+SiO₂
- Acetone
- Isopropyl alcohol
- Photoresist
- KOH Solution
- Distilled water
- Gold target for sputtering
- Conductive paste

Equipment:

- Spinner
- Hot Plate
- UV lamp
- Sputtering machine
- Microscope
- Optical surface profiler Zygo NewView™ 600

Electrodes of a particular geometry intended to be integrated with microchannels in order to perform cell impedance measurement were fabricated through photolithography. Main steps of the process are illustrated in the flux diagram of *Figure 5.1*.

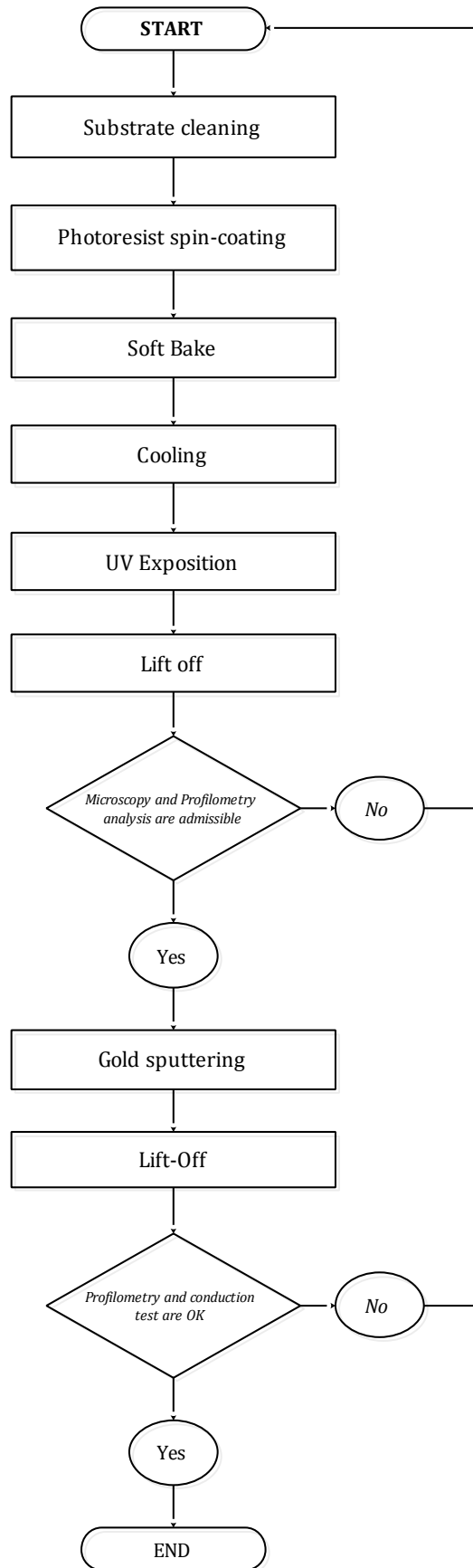


Figure 5.1. Flux diagram of microelectrodes fabrication process.

1) Lithography:

Lithographic main steps are:

- a. **Substrate preparation:** cleaning of the Silicon substrate with acetone and isopropyl alcohol.
- b. **Spin-coating:** resist deposition and spinning. Pre-imposed parameters of the spinner are angular velocity (rpm) and time (s). A positive photoresist was used.
- c. **Soft Bake:** heating on thermal plate.
- d. **Cooling:** couple minutes of cooling at room temperature.
- e. **Development (UV exposition and Lift-off):** selective exposure of the substrate covered by the resist to UV light, using a negative mask. Resist removal by KOH etching followed by washing in distilled water.

2) Gold sputtering

Gold sputtering was performed with a current of 20mA for 220 seconds.

3) Lift-off

Lift-off was done in acetone bath until the desired geometry was obtained.

4) Wire bonding:

Wires were bonded with a conductive paste.

5.1.2 Results and discussion

Results of lithographic process are illustrated in *Figure 5.2* and *Figure 5.3*. Two typologies of electrodes were fabricated: trident-shape and interdigitated. As can be seen, the obtained geometry is the negative shape of the desired electrodes.

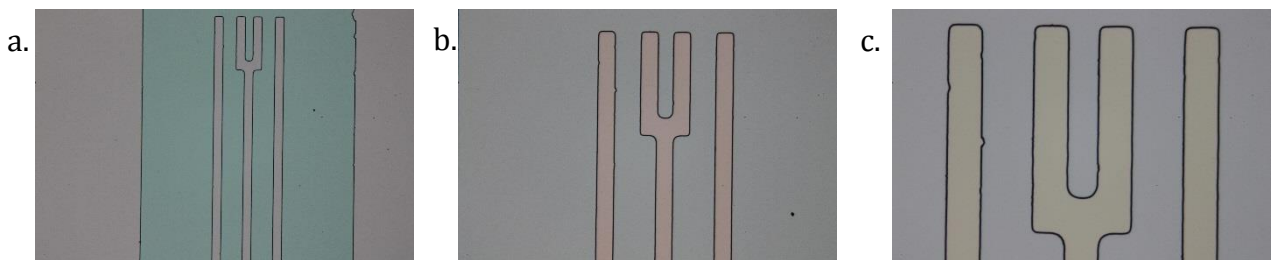


Figure 5.2. Microscopy images of lithographic process outcome. Trident shape a) 5x b) 10x c) 20x.



Figure 5.3. Microscopy images of lithographic process outcome. Interdigitated shape (5x).

Deposited resist height measured by optical profilometry of a sample electrode was $1,99 \mu\text{m}$ (Figure 5.4).

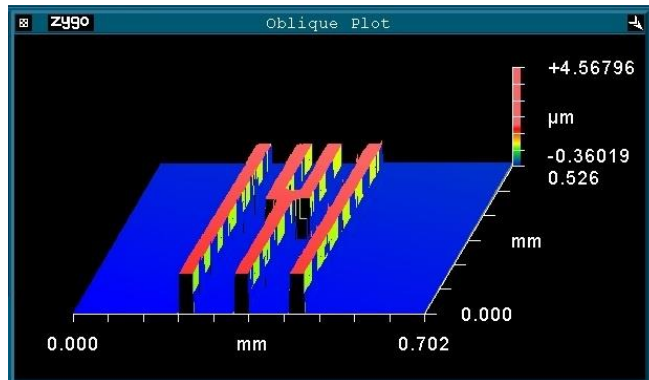


Figure 5.4. Profilometry analysis screenshot of lithographic process outcome. Trident-shape.

Resulting electrodes after sputtering and lift-off are presented in Figures 5.5 and 5.6.

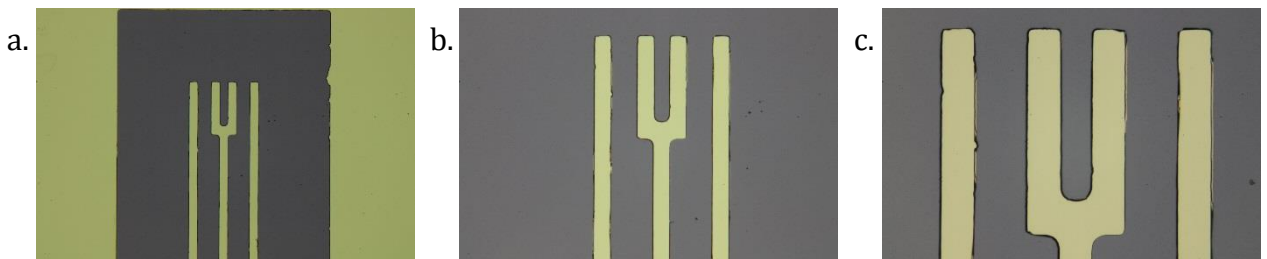


Figure 5.5. Microscopy images of the gold trident-shape electrodes a) 5x b) 10x c) 20x.



Figure 5.6. Microscopy images of the gold interdigitated electrodes (5x).

Main process parameters and characteristics of one sample of a trident shape electrode are summarized in Table 5.1 and Figure 5.7.

Feature	Value
Substrate material	Si + SiO ₂
Electrode material	Au
Spinning angular velocity	2000 rpm
UV exposition time	2 s
Resist thickness after lithography	1,99 μm
Au thickness	0,32 μm

Table 5.1. Main characteristics of the fabricated electrode.

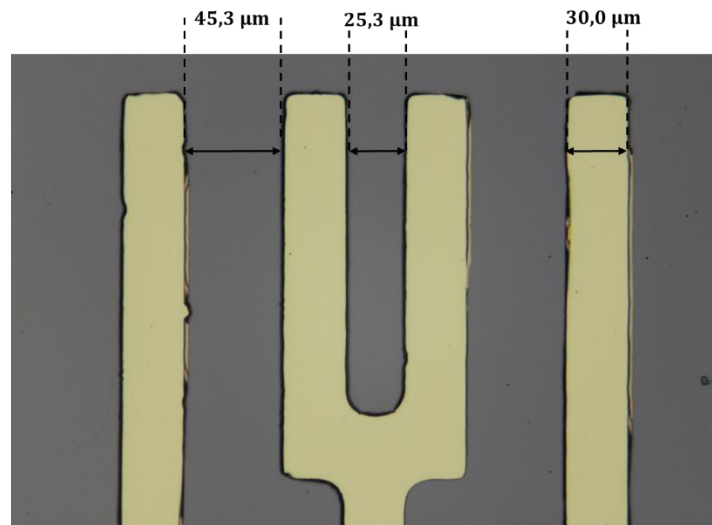


Figure 5.7. Dimensions of the obtained trident-shape electrode.

Dimensions of the obtained interdigitated electrode are presented in Figure 5.8.



Figure 5.8. Dimensions of the obtained interdigitated electrode

Figure 5.9 is a picture of the obtained trident-shape and interdigitated electrodes.

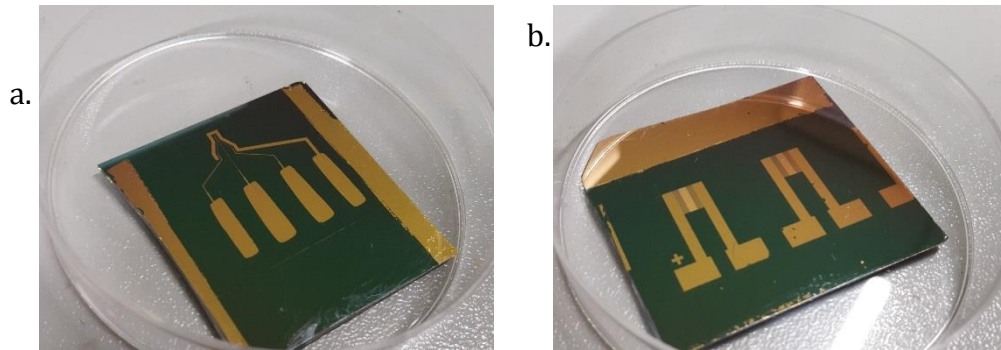


Figure 5.9. a) Trident shape and b) Interdigitated electrodes.

As a final step, wires were bonded to the pads with a conductive paste.

In the lithographic process of gold microelectrodes fabrication, there are multiple critical parameters:

- Spinning angular velocity.
- Soft bake time.
- UV exposure time.
- KOH etching time.
- Sputtering current and time.

Optimization of process parameters is one of the most difficult and time-consuming steps, but is essential for a good throughput.

5.2 Microchannels fabrication

- Objective: fabrication of microchannels masks through a lithographic process for later silicone microchannels fabrication. Microchannels are intended to be integrated with the previously presented microelectrodes for impedance measurement.

5.2.1 Experimental design: material and methods

Materials:

- Substrates: Glass and Si+SiO₂
- Acetone
- Isopropyl alcohol
- Photoresist
- KOH Solution

- Distilled water
- Silicon and hardener

Equipment:

- Spinner
- Hot Plate
- UV lamp
- Weight scale
- Microscope
- Optical surface profiler Zygo NewView™ 600

Microchannels masks were fabricated by photolithography on two different substrates: glass and Si+SiO₂. The obtained masks were then replicated on silicone by casting and finally the microchannels were obtained by photopolymerization. Main steps of the process are illustrated in the flux diagram of *Figure 5.10*.

1) *Lithography:*

Alike the process described in *Section 5.1.1*. Again, a positive resist and a negative mask were used. The output of the lithographic process is a mask with the negative geometry (filled channels).

2) *Silicone casting:*

Starting from the filled channels of the mask obtained by lithographic techniques through a silicone casting the opposite geometry is obtained (empty channels).

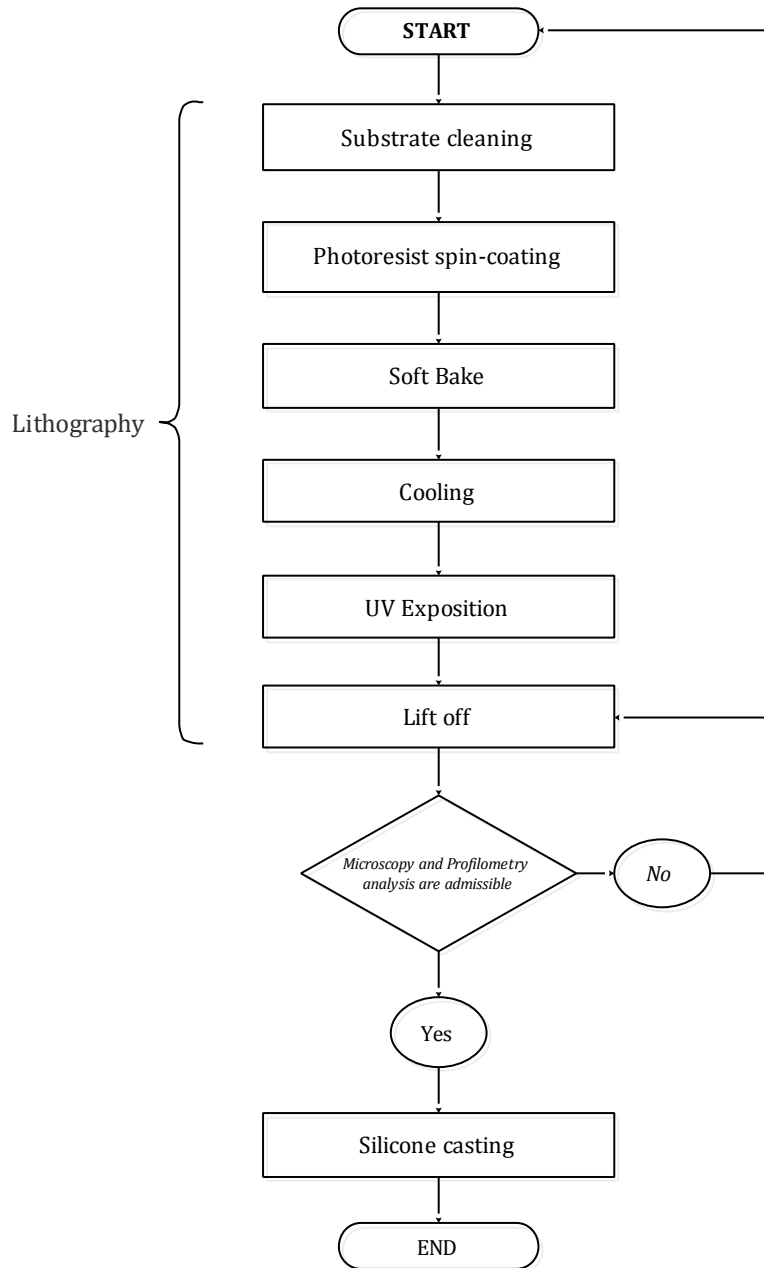


Figure 5.10. Flux diagram of microchannels fabrication process.

5.2.2 Results and discussion

Two main typologies of masks were fabricated: multiple parallel microchannels and a single microchannel. The first one intended to be integrated with the interdigitated electrodes and the second one with the trident-shape electrode.

Multiple parallel microchannels 50 μm width and of two different heights ($\sim 8 \mu\text{m}$ and $\sim 11 \mu\text{m}$) were obtained by the described process. A preliminary flux study was done with yeast cells in blood culture media. The flow, generated by simple capillarity was observed in the microscope as shown in *Figure 5.11*.

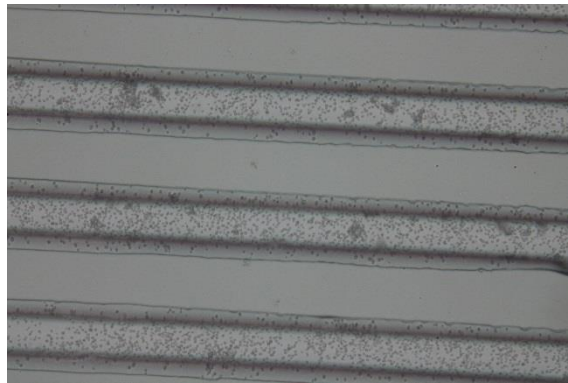


Figure 5.11. Optical microscopy (10X) of yeast cells flowing through 50 μ m width microchannel.

Figure 5.12 is a sequence of images of the fabrication process of the single channel mask. The obtained silicone channel height of 8,59 μ m and a width of 39,5 μ m.

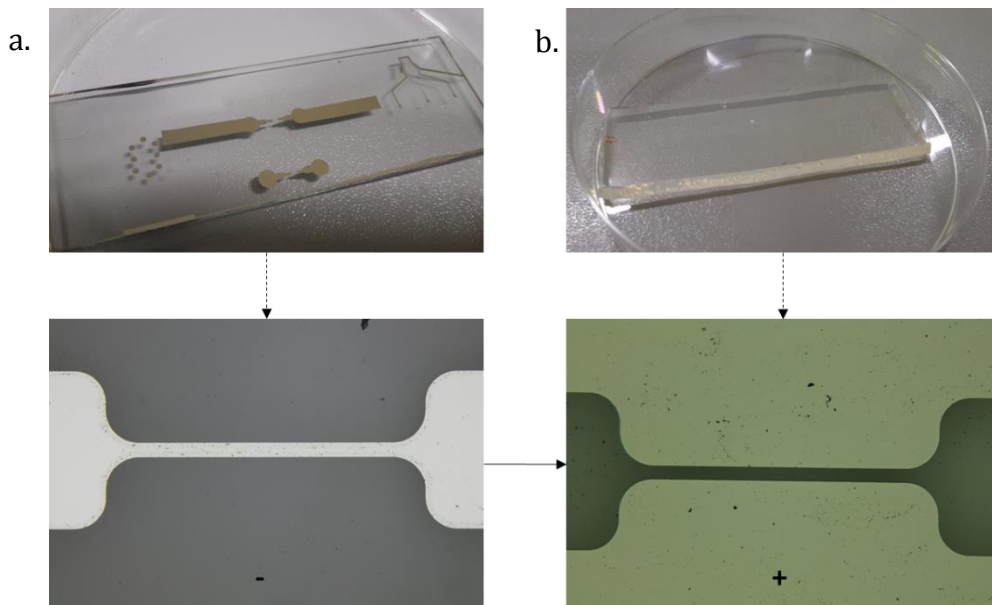


Figure 5.12. Microscopy images of the process (5x). a) Initial mask fabricated by photolithography followed by Cr sputtering and lift-off (filled channel). b) Result of the silicon casting (empty channel).

As expressed in the precedent section, optimization of process parameters is one of the most difficult and time-consuming steps but is essential for a good throughput. In the microchannel fabrication by soft lithography, that uses the Silicone mold, photopolymerization time is the most critical variable.

5.3 Microelectrodes-microchannels integration and impedance measurement

The main objectives are:

- i. To integrate the microchannels with the microelectrodes and identify the potentiality of each configuration.
- ii. To choose, from a multifrequency analysis, a proper frequency for the impedance measurement in the interdigitated electrodes configuration.
- iii. To recognize the differences between impedance measurements done with interdigitated electrodes in mini-wells and in microchannels.
- iv. To study the potentiality of impedance measurement in microchannels.

5.3.1 Experimental design: material and methods

Materials:

- Gold microelectrodes
- Silicon microchannels masks (single and multiple channels)
- Yeast cells in culture medium (Oxoid Signal® Blood Culture System)⁷

Equipment:

- Microscope
- Impedance-meter: Keysight Technologies E4990A impedance analyzer

Microchannels are placed upon previously fabricated microelectrodes for measurement. Two typologies of electrodes and two types of microchannels were used:

- i. Interdigitated electrodes and multiple channels.*
- ii. Trident-shape electrode and single channel.*
- iii. Round interdigitated electrodes.*

Another typology of round interdigitated electrodes of bigger dimensions and fabricated by serigraphy was also used for measurement (*Figure 5.13*). Electrodes were used for impedance measurement of yeast cells under static conditions.

For the measurements with Yeast Cells, 0.2 % KOH solution was added following the protocols found in literature and briefly described in *Section 3.2.1*. By doing so, the CO₂ produced by Yeast metabolism is absorbed by the KOH causing a decrease on the impedance.

⁷ Further information about this culture system can be find in [Section 4.3.1](#)

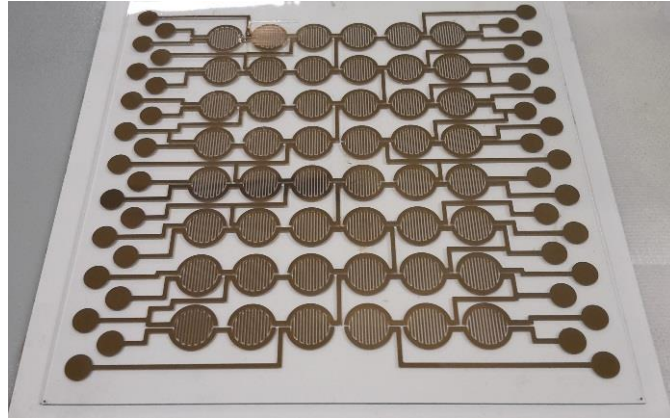


Figure 5.13. Second typology of interdigitated electrodes.

5.3.2 Results and discussion

5.3.2.1 Interdigitated electrodes and multiple channels:

Main features are presented on the experiment chart of *Table 5.2*, and *Figures 5.14 and 5.15* are microscopy images of the system with yeast cells in blood culture medium inside the channels.

Experiment Chart	
Type of electrode	Interdigitated
Electrode material	Aluminum
Type of channel	Multiple channels
Channel width	~50 μm
Channel height	~50 μm

Table 5.2. Experiment chart: interdigitated electrodes and multiple channels.

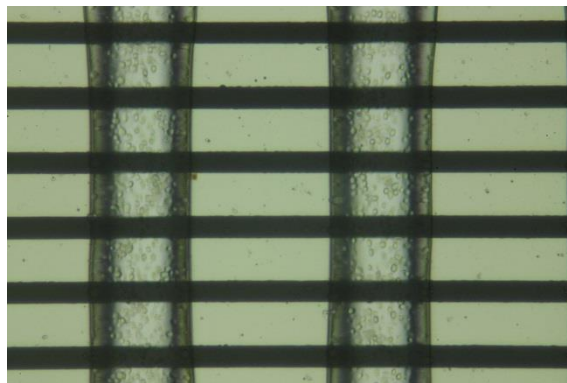


Figure 5.14. Interdigitated electrodes and microchannels with yeast cells inside (20x).

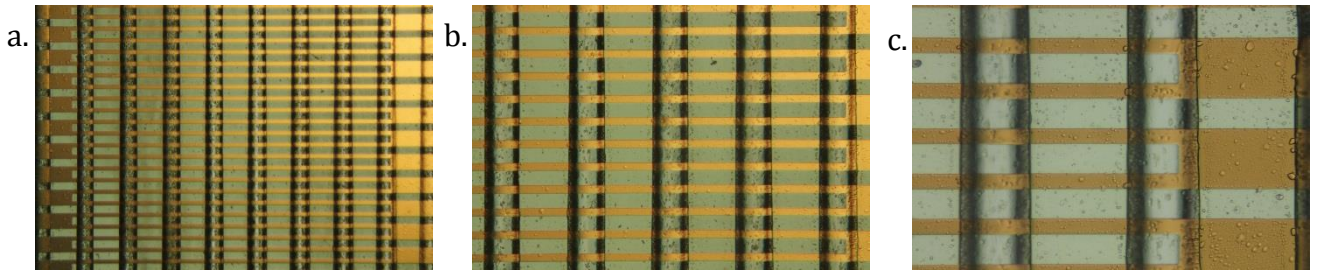


Figure 5.15. Interdigitated electrodes and microchannels seen at the microscope illuminating the back surface of the sample (transmitted illumination). a) 5x. b) 10x. c) 20x.

A first measurement, with the scope of understanding the impedance order of magnitude, consisted on evaluating the impedance variation when the channels were filled with culture medium under static conditions. Nominal impedance of the system with empty channels was around $\sim 800 \text{ M}\Omega$ and upon deposition of a drop of blood culture medium an instantaneous reduction to $\sim 40 \text{ M}\Omega$ was observed. Later, when the channels were completely filled, and the flux stopped, the obtained impedance reading was $\sim 10 \text{ M}\Omega$.

Further experiments with this configuration are needed to understand the measurement potential of the system. The incapability of reusing the electrodes because of the absence of an external flux inducer, and the time-consuming electrodes process fabrication gives to this experimental set-up a low throughput.

5.3.2.2 Trident-shape electrode and single channel:

Main features are presented on the experiment chart of Table 5.3, and Figure 5.16 is a microscopy image of the system.

Experiment Chart	
Type of electrode	Trident-Shape
Electrode material	Gold
Type of channel	Single channel
Channel width	$\sim 39,5 \mu\text{m}$
Channel height	$\sim 8,59 \mu\text{m}$

Table 5.3. Experiment chart: trident-shape electrode and single channel.

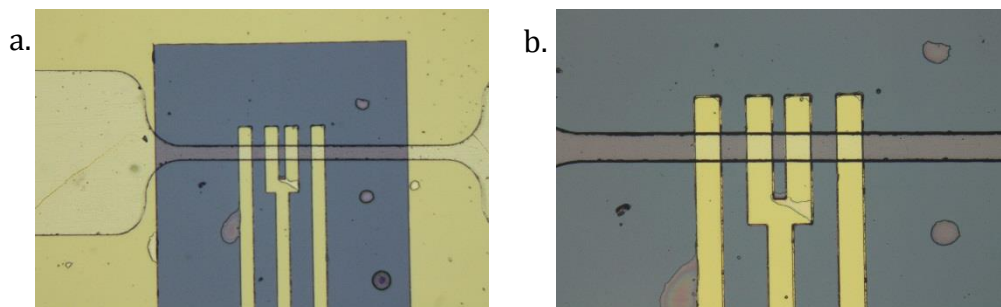


Figure 5.16. Trident shape electrode and single microchannel a) 5x b) 10x

In *Figure 5.17* is presented a sequence of images that show the microchannel filling process with yeast cells in blood culture medium by capillarity. The fluid took a couple of seconds to reach the channel, once filled a fast flux is trigger. All the presented images represent a time-lapse of less than a minute.

The electrode configuration and the use of a single channel has a great potential for measurements of flowing entities in a flux regime. Such a set-up, with the correspondent dimension adjustments, could be used, for example, as a cell counting system.

With the aim to exploit the potential of the configuration for a time-dependent impedance measurement under flux conditions, measurement was performed by means of a tension variation in the electrode terminal with an oscilloscope. However, attempts to measure impedance with this configuration were not successful because of the presence of excessive noise. A proper acquiring system needs to be implemented for a proper time-dependent measurement.

A similar experimental set-up, with coplanar electrodes of similar characteristics, was performed by Claudel J *et al.* In their study test were carried with calibrated beads, yeast cells and red blood cells [33].

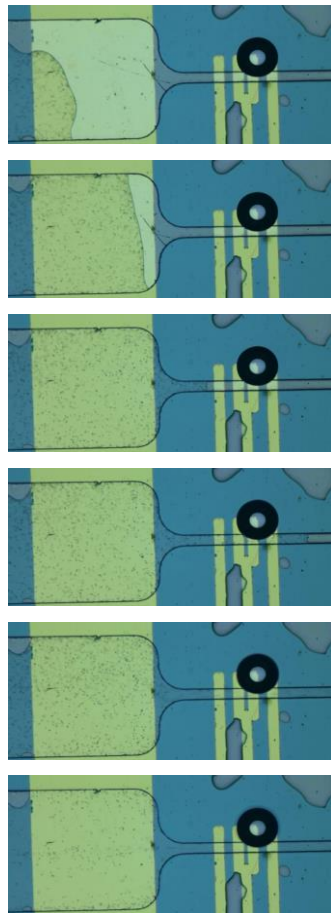


Figure 5.17. Sequence of images of the microchannel filling process.

5.3.2.3 Round interdigitated electrodes:

Electrodes geometry and dimensions are presented in *Figure 5.18*.

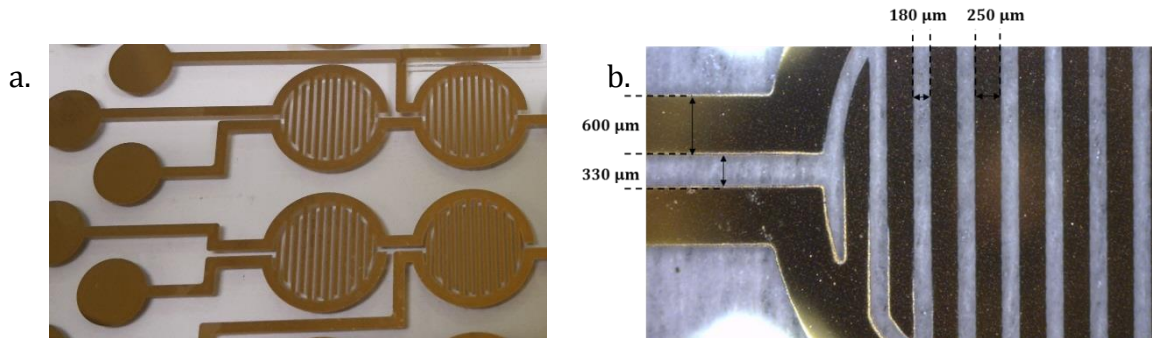


Figure 5.18. a) Geometry and b) dimensions of the round interdigitated electrodes.

This typology of electrode was used for yeast cell impedance measurement under static conditions. Two typologies of impedance measurements of yeast cells in blood culture medium were done: mini-well and microchannels. Both systems, mini-well and microchannels were then tested both with the impedance-meter and with a suitable simultaneous acquisition system that will be later described.

List of experimental tests:

- Mini-well with impedance-meter.
- Mini-well with simultaneous acquisition system.
- Microchannels with impedance-meter.
- Microchannels with simultaneous acquisition system.

Impedance measurement with the impedance-meter and the mini-well configuration was done for more than an hour (~ 70 minutes) and for 3 different samples: blood culture medium and yeast cells in blood culture medium at two different concentrations (45% and 81%). It is important to clarify that these concentrations are nominal values because the starting yeast population is not quantitatively known.

Leaving aside time dependency for a while in order to study global impedance behavior in the chosen frequency range (multifrequency study), analysis was performed with the mean impedance value. *Figure 5.19* corresponds to the mean of all the curves acquired at different time instants for the three samples. *Figure 5.20* is a zoom of the previous figure in the frequency window from 1 kHz to 10 kHz.

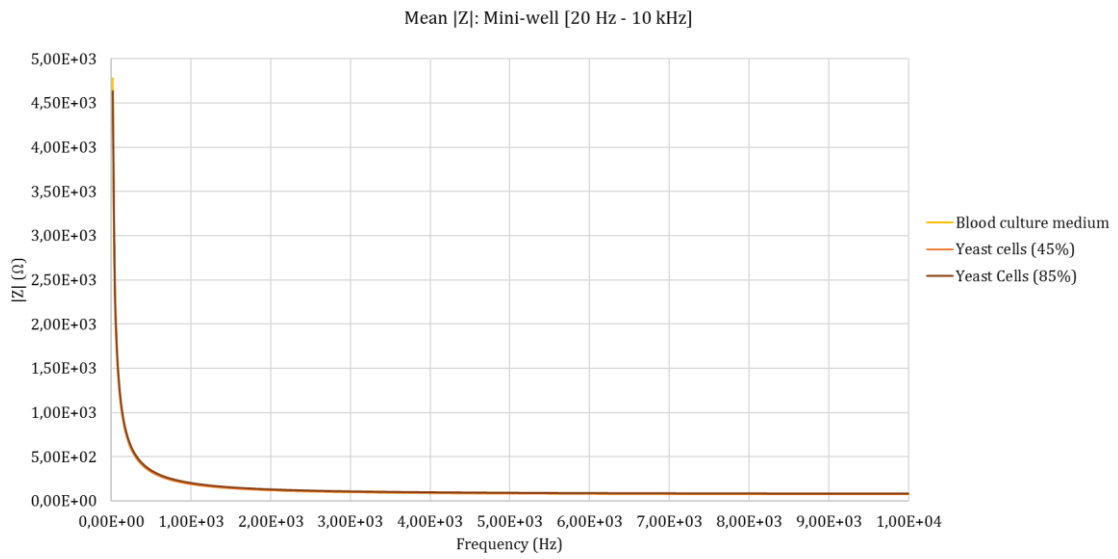


Figure 5.19. Mean $|Z|$ curve in the frequency range from 20 Hz - 10 kHz for mini-well measurement of the three samples.

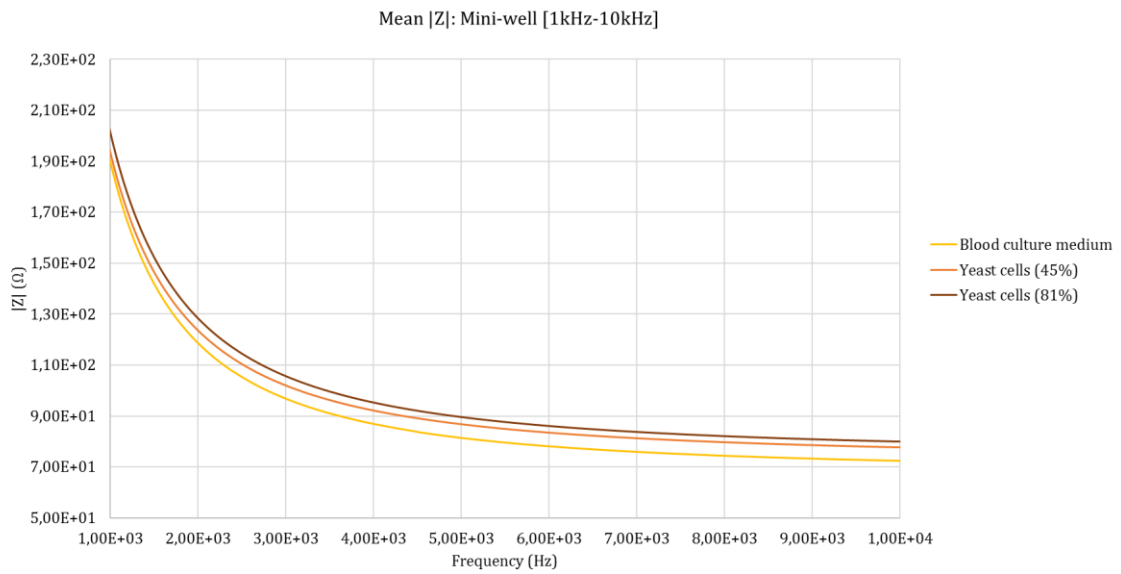


Figure 5.20. Mean $|Z|$ curve in the frequency range from 1 kHz - 10 kHz for mini-well measurement of the three samples.

From Figure 5.20 it can be immediately implied that the presence of yeast cells in culture medium causes a global increase on impedance magnitude.

Involving the time variable, very little variations in the measured impedance during an hour were observed, *Figure 5.21* is the $|Z|$ - θ plane in which data points correspond to measurements at selected frequencies at a different time instant. Three frequencies were analyzed: 1 kHz, 5 kHz and 10 kHz. The arrows in the graph represent the time as they indicate the direction in which data points must be read going from the “time-zero” measurement to the final measurement. As expected, very little variation of impedance magnitude in time is observed for blood culture medium at the three observed frequencies (points follow an almost horizontal line).

Considering the phase two different time-dependent phenomena are observed. At 1 kHz the phase increases while at higher frequencies (5 kHz and 10 kHz) the phase decreases. For the impedance modulus, a tendency to increase is observed for all the studied frequencies.

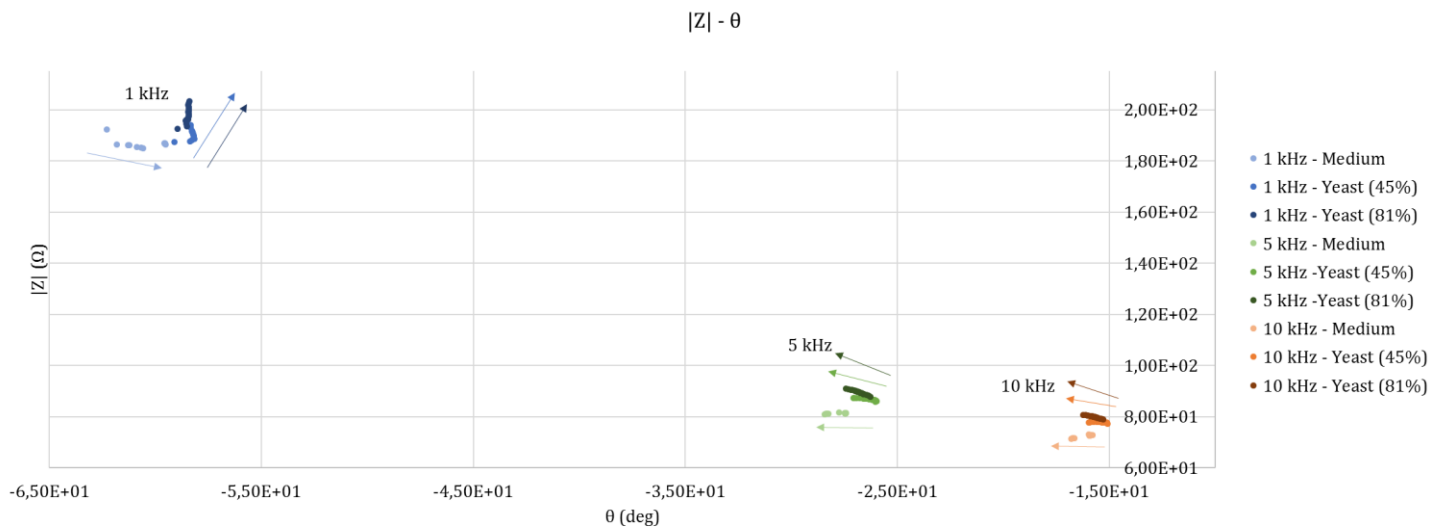


Figure 5.21. $|Z|$ - θ Plane for measurements for about an hour for 3 different frequencies: 1 kHz, 5 kHz and 10 kHz. Arrows are indicators of time (initial and final data point).

For further impedance analysis, data at 10 kHz was selected. The choice was made based on several reasons. As explained in *Section 3.2*, at intermediate frequencies the polarization phenomenon is reduced and, as suggested by *Posseckardt et al.*, for frequencies from 10 kHz onwards the spectrum is dominated by the resistance of the solution at the electrode interface [26]. On the other hand, the acquisition system developed at the company that will be described below, allows impedance measurement at 200 Hz and 10 kHz and therefore, in order to be able to do a measurement subjected to comparison, 10 kHz was chosen.

Impedance measurement with the impedance-meter in micro-well at 10 kHz is presented in *Figure 5.22*. Measurement was done for 21 minutes⁸.

⁸ Samples are taken every 3 minutes. In *Figure 5.22*, are presented 8 measurements that correspond therefore to a 21 minutes long registration (first measurement at $t_i=0$).

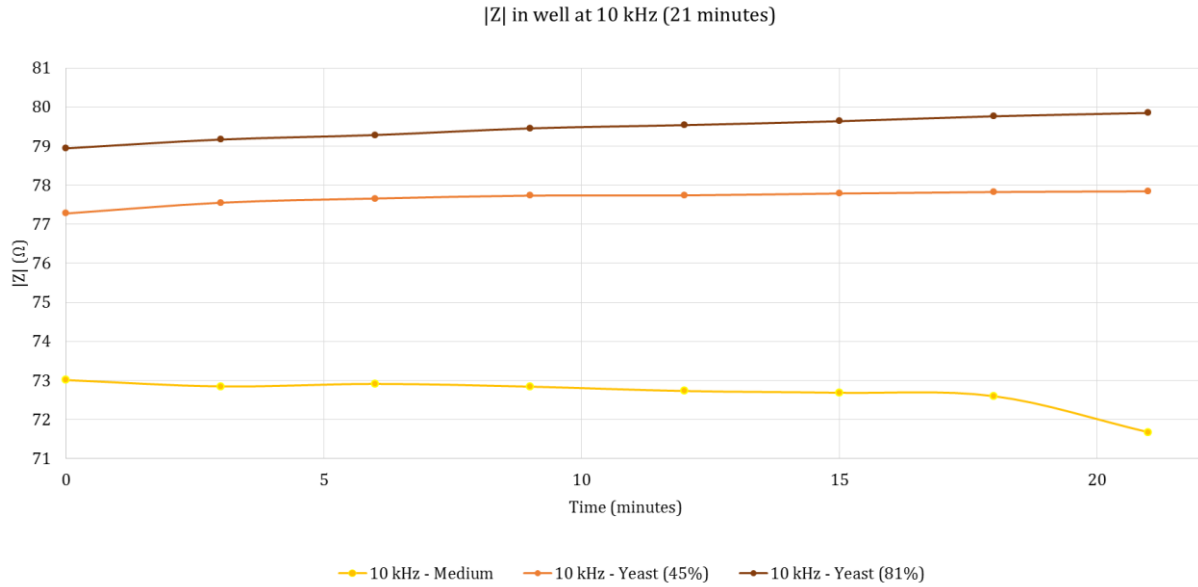


Figure 5.22. Impedance measurement in well at 10 kHz for 21 minutes acquired with the impedance-meter. Yeast at two different concentrations and blood culture medium.

Well impedance measurements were repeated with a suitable acquisition system designed and developed at the Company **Eltek. S.p.A** that allows the simultaneous measurement of multiple samples (Figure 5.23). The system allows the parallel measurement of 48 interdigitated electrodes and sends data directly to a computer through a USB⁹ cable. It performs impedance measurement at two different frequencies: 200 Hz and 10 kHz. Advantages of this acquisition system are the parallel acquisition, direct data visualization and saving on PC, sampling at precise time intervals, facility for a long-term measurement, reduction of human error and reduction in data processing time. Impedance measurement analysis was performed at 10 kHz.



Figure 5.23. Experimental set-up of the acquisition system used for simultaneous impedance measure in wells.

⁹ USB: Universal Serial Bus

Three yeast samples were used: blood culture medium without cells, a supersaturated yeast cells solution in medium and a solution of the precedent one diluted to around its 50%. In *Figure 5.24* are identified as high concentration and low concentration yeast. Measurement was performed for 119 minutes¹⁰.

In *Figure 5.24*, it can be observed that blood culture medium shows a gradual impedance reduction, while in the yeast samples two phenomena were observed: a first increase in impedance followed by a gradual reduction. The phenomena is more accentuated on the most concentrated yeast sample but is present in the two yeast samples.

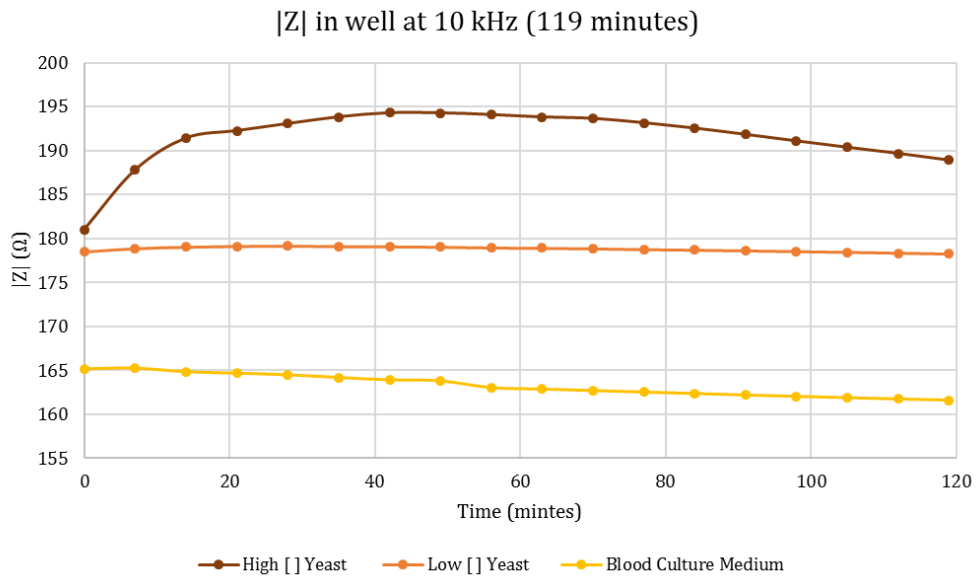


Figure 5.24. Impedance measurement in well at 10 kHz for 119 minutes acquired simultaneously for yeast at two different concentrations and blood culture medium.

Main features of the impedance measurement with microchannels are presented on the experiment chart of *Table 5.4*.

Figure 5.25 is a microscopy image of the system in two conditions: empty channels (a) and with yeast cells in blood culture medium inside the channels (b).

¹⁰ Samples are taken every 7 minutes. In *Figure 5.24*, are presented 18 measurements that correspond therefore to a 119 minutes long registration (first measurement at $t_i=0$).

Experiment Chart	
Type of electrode	Round interdigitated
Electrode material	Gold
Type of channel	Multiple channels
Channel width	~50 μm
Channel height	~8 μm

Table 5.4. Experiment chart: round interdigitated electrodes and multiple channels.

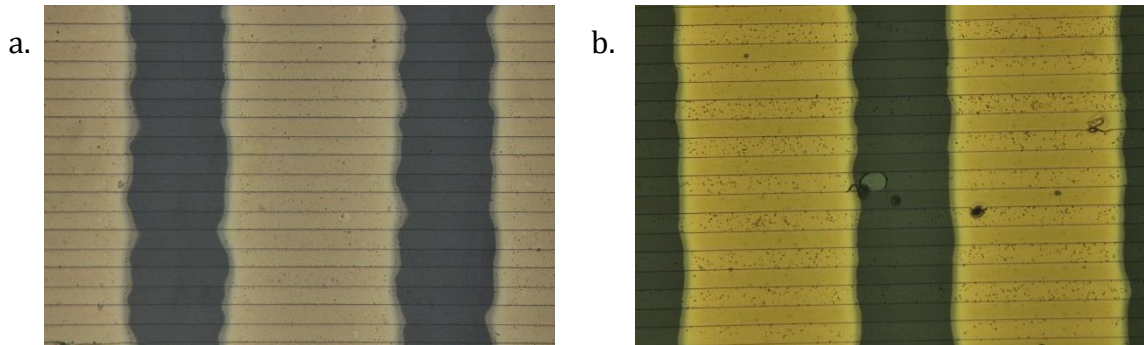


Figure 5.25. Round interdigitated electrodes and microchannels (5x) with a) empty channels and b) yeast cells in blood culture medium.

Impedance measurement with the impedance-meter in microchannels was done for two samples: blood culture medium and yeast cells. Measurements were done for 27 minutes¹¹ and for data comparison with the precedent set-up in well, the analysis was carried at a frequency of 10 kHz (Figure 5.26).

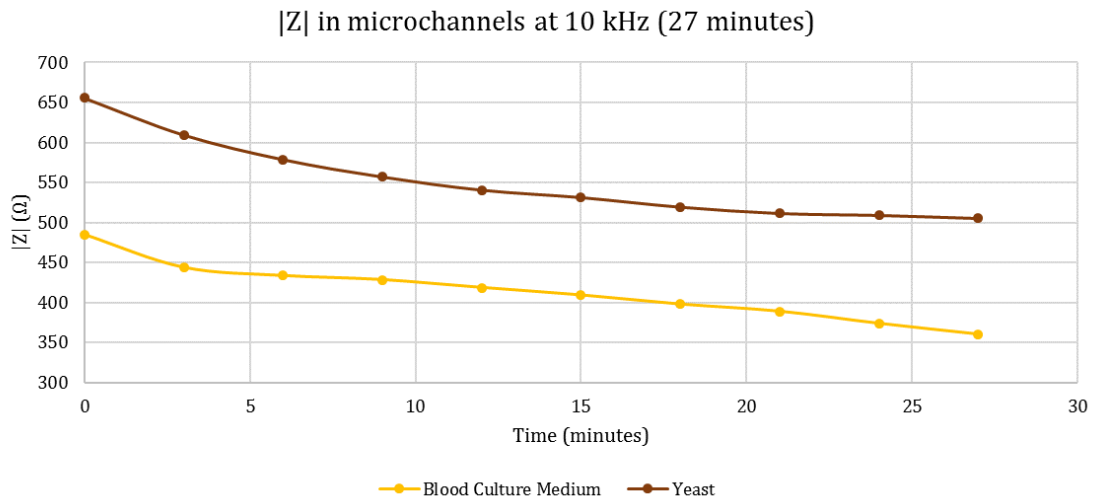


Figure 5.26. Impedance measurement in microchannels at 10 kHz for 27 minutes acquired with the impedance-meter. Yeast and blood culture medium.

¹¹ Samples are taken every 3 minutes. In Figure 5.26, are presented 10 measurements that correspond therefore to a 27 minutes long registration (first measurement at $t_i=0$).

From Figure 5.26, that corresponds to microchannel impedance measurement, and Figure 5.22, that illustrates well impedance measurement, both acquired with the impedance-meter in a similar time interval, a direct relation between impedance and cell concentration is observed. For both configurations, the higher the concentration, the higher is the measured impedance, however, a completely opposite curve tendency is observed. Microchannels measurements show a gradual impedance reduction from the first acquired data point. Well impedance, on the other hand, show impedance increase in this time interval, impedance diminution takes place after several minutes (after the first half hour). A hypothesis of the first impedance increase in the well case is the decanting of yeast cells on the bottom of the well (electrode surface). As the microchannels have a low height this phenomenon does not take place. In literature, other reports of this phenomena can be found. *J.J Lieu et al.*, report that one of the problems when measuring impedance of cells in suspension is the formation of aggregates on the surface of the electrode that may disturb the impedance measurement. To overcome this problem, they propose the deposition of a thin film of agarose [34].

Microchannels impedance measurements were also repeated with the simultaneous acquisition system described before at 10 kHz and for 119 minutes. Four samples were tested: blood culture medium without cells, a supersaturated yeast cells solution in medium (100%), a solution of the precedent one diluted to its 50%, and another dilution at the 10%. In Figure 5.28, are identified as high, medium and low concentration yeast.

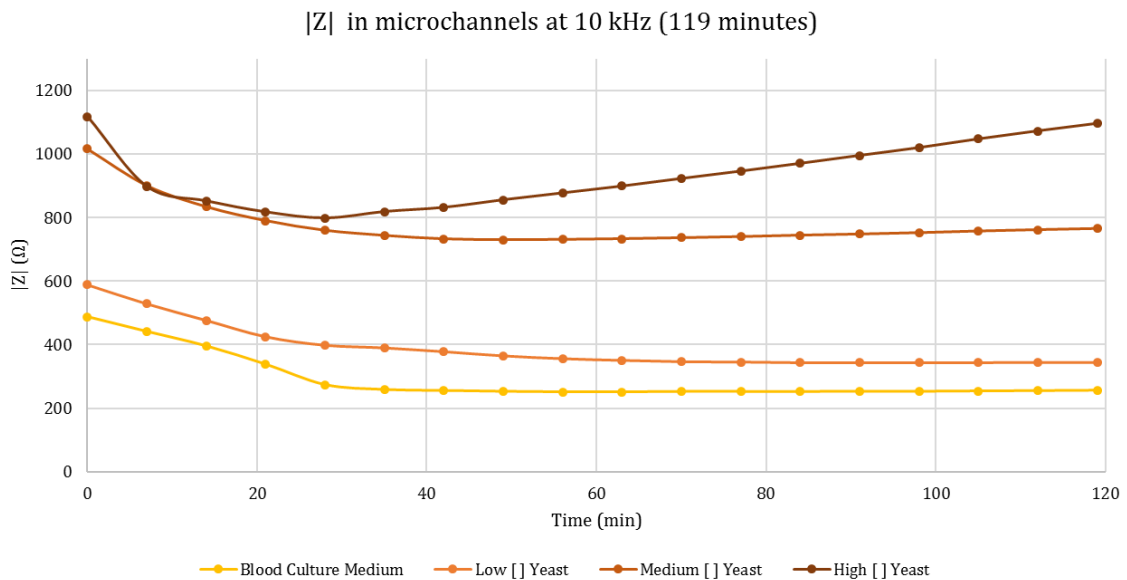


Figure 5.27. Impedance measurement in microchannels at 10 kHz for 119 minutes acquired simultaneously for yeast at three different concentrations and blood culture medium.

For analysis purposes in Figure 5.29, both well and microchannels measurements are shown. It is important to clarify that well and microchannels concentrations

are not the same, they must be analyzed in terms of trend or in comparison between measurements of the same type (well or microchannel).

As observed in the data obtained with the impedance-meter, microchannel measurements show an immediate reduction while measurements in the well experiment first an impedance increase, mainly attributed to deposition of yeast on the electrode surface. *Figure 5.29* makes evident that measurements in microchannels show a greater impedance variation.

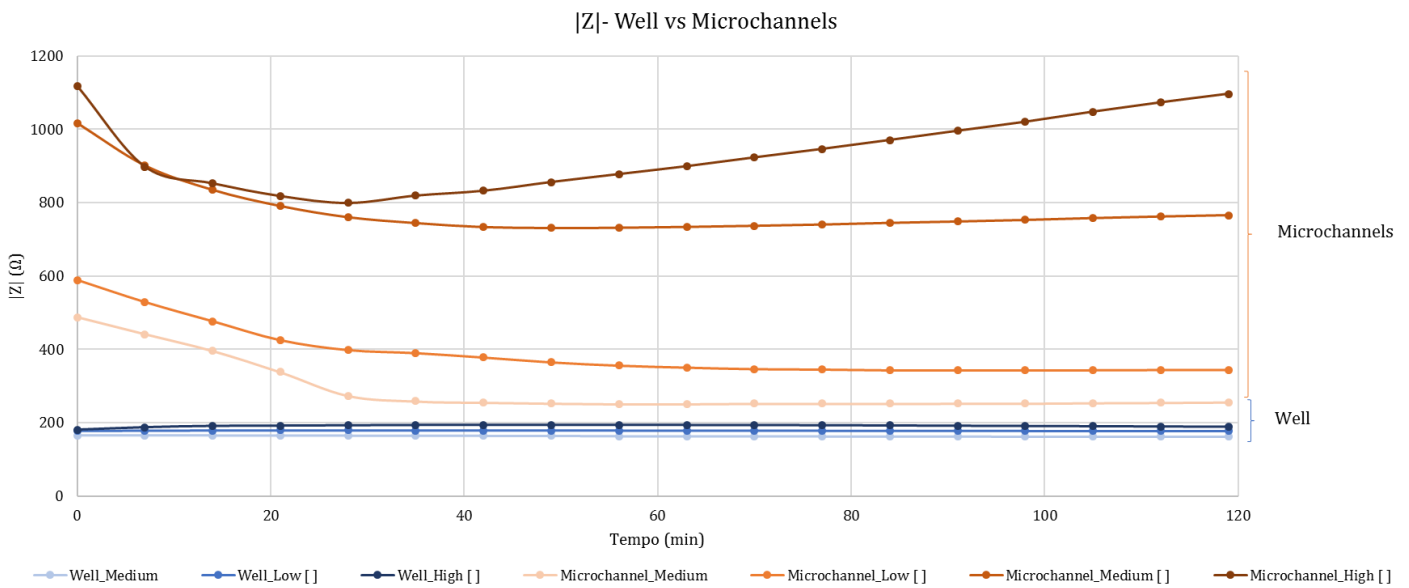


Figure 5.28. Impedance measurement in well and in microchannels at 10 kHz for 119 minutes.

As mentioned before, impedance measurement serves as a vitality indicator with yeast cells. The methodology defines the “detection time” as the time taken to reach a certain impedance change value ([29]–[31]). For microchannels measurement, the time taken to reach the minimum could be of interest as it is an inverse indicator of yeast concentration. Minimum impedance value is reached in the following times:

- High concentration yeast (100%): 28 minutes.
- Medium concentrated yeast (50%): 49 minutes.
- Low concentrated yeast (10%): 91 minutes.

Here the minimum impedance value is hypothesized to be when the KOH present in the solution is exhausted. However, underlying chemical and biological phenomena needs to be further studied to affirm it.

Normalizing microchannels yeast measurements to the culture medium shows that most significant impedance changes take place during the first half hour (*Figure 5.30*).

As measurement in short-time periods could be of interest for some applications, measurements in microchannels, in comparison with the well measurements, solves the problem of aggregates formation on the electrode surface and seem to have the potential for measuring time reduction and enhanced sensibility. However further experiments are needed to confirm the hypothesis and better understand the measured phenomena.

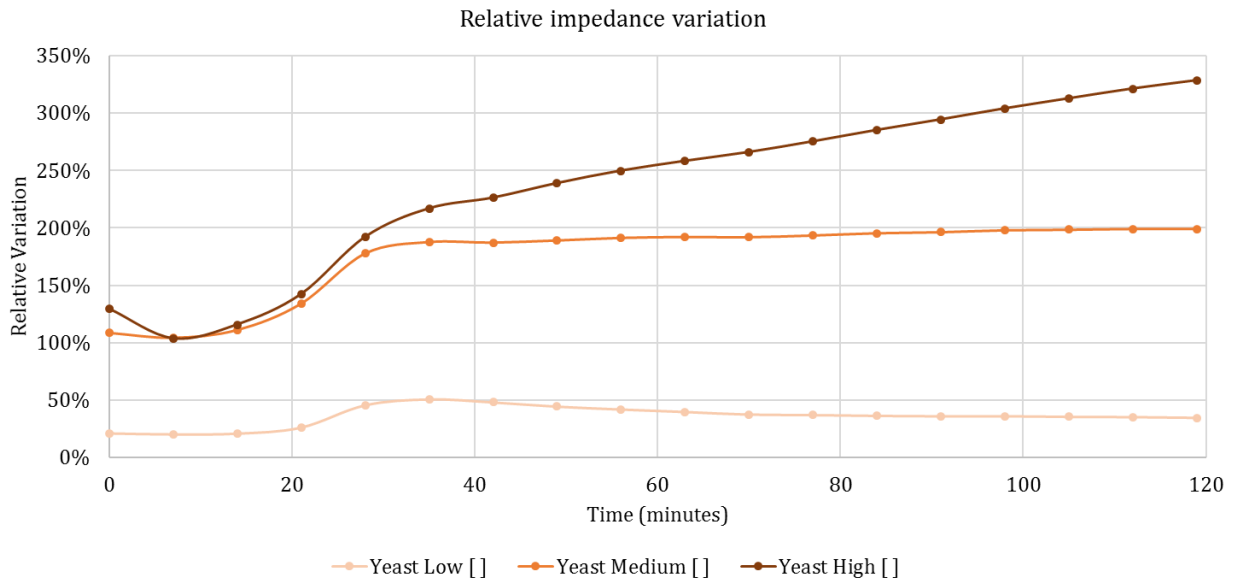


Figure 5.29. Relative impedance variation (normalized to Blood Culture Medium).

In all the systems previously presented, as the flux flows by capillarity without a pumping mechanism, they can be used just once, limiting it to a single measurement and leading to the incapability to perform control measurements with the exact same electrode. The development of a microfluidic pumping system is strongly suggested.

Conclusions and future perspectives

For the first part, M4N measurements showed, from a global point of view, coherent results between them. A relation between gap distance and sensibility can be inferred as measurements of “Up” couples of electrodes, that have the smaller gap distance (2,5 μm), presented a greater variation.

Experimental data strongly evidences that using the M4N without a nanostructured material between the electrodes is very likely to go out of the measuring range. As the acquired data was out of R and C range and data analysis was carried in terms of T_0 and T_1 is not possible to come out with outright conclusions to affirm if the platform is suitable for measurement in aqueous environments, and therefore for cellular biology applications.

For further experimentation and tests, metallization of the electrodes is strongly suggested, as proposed by *Miccoli. B* by means of the Electroless Nickel Immersion (ENIG) technique in [5].

From the presented data, different alternatives emerge for further analysis:

- i. Perform further tests in terms of T_0 and T_1 in order to understand if these two variables offer substantial information for the target application, without the need of their conversion to electric variables.
- ii. Find a new mathematical model that allows T_0 and T_1 conversion into R and C in a wider range.
- iii. Propose a new ROC for the target application.
- iv. Propose other sensing applications using the M4N with ZnO nanowires or another nanostructured material, as it was thought at the beginning when the platform was designed.

A very interesting and still little studied path is the potentiality of the DEP¹² circuits of the M4N platform for alternative biological applications. Advantages of the DEP circuit implemented is the possibility to set the frequency in a range from 50 kHz to 1 MHz. A further study to exploit the DEP potential of this systems is suggested to be preceded by the determination of DEP parameters by analytical methods.

As mentioned at the beginning of this thesis, it is worth to highlight that features of the M4N such as integrated microelectronics (already optimized for parasitics reduction and low-noise measurement), interface with commercial electronics

¹² Dielectrophoresis

(Arduino Due), implemented graphic user interface (GUI) for real time acquisition and multi-nanosensor capability make the platform attractive for multiple applications, and the results of the presented experiments should be considered just as an outline, as the first step of a long path of explorations with this system.

For the second part, in the presented fabrication processes there are multiple critical parameters. Optimization of these parameters is time-consuming but is essential for having a good throughput, reproducible results and therefore a possibility for scaling-up the processes.

For the trident-shape electrode configuration, in order to take advantage of the geometry and the possibility of performing a single channel measurement, an appropriate signal acquiring system should be implemented. This system has the potential for single cell impedance measurement by means of downscaling the channel to dimensions comparable with the cell of interest. By doing so, the system could be used for cell counting.

For the test conducted with the interdigitated electrodes, a direct relation between yeast concentration and impedance was observed. For all the experimental set-ups, the higher the yeast concentration the higher was the measured impedance. To perform the measurement with two different instruments, impedance-meter and the described simultaneous acquisition system, allows to validate the Company's system and gives more robustness to the presented data.

Results obtained with the interdigitated electrodes and microchannels are attractive in terms of time reduction, enhanced sensibility, and reduction of the aggregates formation on the electrode surface phenomenon. Further tests to understand differences between well and microchannels measurements behavior and studies on the microchannel height dependency could be a following step.

In general, the development of a pumping system is suggested to be able to use the same electrode for different tests and controlling flux parameters.

The multi-channel simultaneous acquisition system presented in the last part opens the possibility for a great number of different contemporary measurements.

Once understood the physical/biological phenomenon beneath this impedance measurements, tests with different typologies of cells could be conducted.

A. Figures Index

Figure 0.1. Scopus publications per year about “biosensing AND cells AND Impedance”. [4].....	11
Figure 1.1. M4N complete system.....	15
Figure 1.2. M4N fabrication flow (Figure from [5]).	16
Figure 1.3. Schematic representation of NWs alignment by DEP (Figure from [6]).	18
Figure 1.4. Schematic of the Quasi-Digital Impedance Converter (QDIC) (Figure from [9]).	19
Figure 1.5. Calibration flow diagram for R and C calculation. (Diagram adapted from [6]).	21
Figure 1.6 LabVIEW GUI main page screenshot.	22
Figure 2.1. Microfabrication technologies (Scheme information from [13]).	25
Figure 2.2. Surface profile measurement techniques summary scheme (Scheme information from [21]).	29
Figure 3.1. a) Single-Shell model. b) Double-Shell model (Image adapted from [22]).	31
Figure 3.2. Electrical model of a single cell in suspension (Image adapted from [24]).	32
Figure 4.1. Flux diagram of the M4N assembly process.	35
Figure 4.2. Assembled M4N ready for testing.	36
Figure 4.3. Optical microscopy of M4N a) Eight SoC (5x) with the standard cell numeration. b) 10x c) Two M4N cells in which up, middle and down electrodes are identified (20x).	37
Figure 4.4. Flux diagram of the executed calibration process.....	39
Figure 4.5. Impedance measurement in well.....	43
Figure 4.6. T ₀ -T ₁ Plane with all the measurements.....	43

Figure 4.7. T ₀ and T ₁ Box and Whiskers plots for all the measurements.	44
Figure 4.8. T ₀ -T ₁ Plane with measurements for blood culture medium and yeast cells.....	44
Figure 4.9. Microscopy images of a) cell 3 and b) cell 8. In both cases oxidation is observed in one of the middle electrodes.	45
Figure 4.10. T ₀ and T ₁ relative variation of cells “Up” and “Down”	45
Figure 4.11. T ₀ values for ALTE _{down} of cell 4 for 300 samples.....	46
Figure 4.12. T ₁ values for ALTE _{down} of cell 4 for 300 samples.....	46
Figure 4.13. T ₀ and T ₁ for “Up” couple of electrodes.	47
Figure 4.14. T ₀ and T ₁ for “Middle” couple of electrodes.....	47
Figure 4.15. T ₀ and T ₁ for “Down” couple of electrodes.	48
Figure 4.16. Relative variation of T ₀ and T ₁ with and without gold nanoclusters.	48
Figure 4.17. Impedance measurement curves for the 4 solutions (frequency axis in logarithmic scale).	49
Figure 4.18. Impedance measurements of interdigitated gold electrodes in the range [100 Hz – 100 kHz]	50
Figure 4.19. Impedance measurement curves for blood culture medium with and without yeast cells in the frequency range from 100 Hz to 100 kHz (frequency axis in logarithmic scale).	50
Figure 5.1. Flux diagram of microelectrodes fabrication process.	53
Figure 5.2. Microscopy images of lithographic process outcome. Trident shape a) 5x b) 10x c) 20x.	54
Figure 5.3. Microscopy images of lithographic process outcome. Interdigitated shape (5x).	54
Figure 5.4. Profilometry analysis screenshot of lithographic process outcome. Trident-shape.....	55
Figure 5.5. Microscopy images of the gold trident-shape electrodes a) 5x b) 10x c) 20x.	55
Figure 5.6. Microscopy images of the gold interdigitated electrodes (5x).....	55
Figure 5.7. Dimensions of the obtained trident-shape electrode.	56
Figure 5.8. Dimensions of the obtained interdigitated electrode	56
Figure 5.9. a) Trident shape an b) Interdigitated electrodes.....	57

Figure 5.10. Flux diagram of microchannels fabrication process.....	59
Figure 5.11. Optical microscopy (10X) of yeast cells flowing through 50µm width microchannel.....	60
Figure 5.12. Microscopy images of the process (5x). a) Initial mask fabricated by photolithography followed by Cr sputtering and lift-off (filled channel). b) Result of the silicon casting (empty channel).....	60
Figure 5.13. Second typology of interdigitated electrodes.....	62
Figure 5.14. Interdigitated electrodes and microchannels with yeast cells inside (20x).....	62
Figure 5.15. Interdigitated electrodes and microchannels seen at the microscope illuminating the back surface of the sample (transmitted illumination). a) 5x. b) 10x. c) 20x.	63
Figure 5.16. Trident shape electrode and single microchannel a) 5x b) 10x.....	63
Figure 5.17. Sequence of images of the microchannel filling process.....	64
Figure 5.18. a) Geometry and b) dimensions of the round interdigitated electrodes.....	65
Figure 5.19. Mean $ Z $ curve in the frequency range from 20 Hz – 10 kHz for mini- well measurement of the three samples.....	66
Figure 5.20. Mean $ Z $ curve in the frequency range from 1 kHz – 10 kHz for mini- well measurement of the three samples.....	66
Figure 5.21. $ Z $ - θ Plane for measurements for about an hour for 3 different frequencies: 1 kHz, 5 kHz and 10 kHz. Arrows are indicators of time (initial and final data point).....	67
Figure 5.22. Impedance measurement in well at 10 kHz for 21 minutes acquired with the impedance-meter. Yeast at two different concentrations and blood culture medium.	68
Figure 5.23. Experimental set-up of the acquisition system used for simultaneous impedance measure in wells.	68
Figure 5.24. Impedance measurement in well at 10 kHz for 119 minutes acquired simultaneously for yeast at two different concentrations and blood culture medium.....	69

Figure 5.25. Round interdigitated electrodes and microchannels (5x) with a) empty channels and b) yeast cells in blood culture medium.....70

Figure 5.26. Impedance measurement in microchannels at 10 kHz for 27 minutes acquired with the impedance-meter. Yeast and blood culture medium.70

Figure 5.27. Impedance measurement in microchannels at 10 kHz for 119 minutes acquired simultaneously for yeast at three different concentrations and blood culture medium.71

Figure 5.28. Impedance measurement in well and in microchannels at 10 kHz for 119 minutes.72

Figure 5.29. Relative impedance variation (normalized to Blood Culture Medium).73

B.Tables Index

Table 1.1. Overview of the M4N main features.....	15
Table 1.2. Main M4N serial commands.	23
Table 4.1. T_0 and T_1 for $C_{add}= 0$ pF. T_0 values for different C_{add}	39
Table 4.2. Sensitivity calculation.	40
Table 4.3. Mean sensitivity, C_{base} and R_{par}	40
Table 4.4. Obtained R and C for 3 different simulated R values and the systematic error, with $a=12$ and assuming the simulated C as zero.	40
Table 4.5. Calibration parameters.....	41
Table 5.1. Main characteristics of the fabricated electrode.	56
Table 5.2. Experiment chart: interdigitated electrodes and multiple channels.....	62
Table 5.3. Experiment chart: trident-shape electrode and single channel.	63
Table 5.4. Experiment chart: round interdigitated electrodes and multiple channels.....	70

Bibliography

- [1] G. M. Walker, J. M. Ramsey, R. K. Cavin, D. J. . Herr, C. I. Merzbacher, and V. Zhirnov, "A Framework for Bioelectronics: Discovery and Innovation," 2009.
- [2] A. N. Sekretaryova, M. Eriksson, and A. P. F. Turner, "Bioelectrocatalytic systems for health applications," *Biotechnol. Adv.*, vol. 34, no. 3, pp. 177–197, 2016.
- [3] K. Lei, P. Mak, M. Law, and R. P. Martins, "CMOS biosensors for in vitro diagnosis: transducing mechanisms and applications," *Lab Chip*, vol. 16, pp. 3664–3681, 2016.
- [4] "Scopus - Analyze search results." [Online]. Available: <https://www-scopus-com.ezproxy.biblio.polito.it/term/analyzer.uri?sid=f62301556ff0d311374096d29373b7a7&origin=resultslist&src=s&s=TITLE-ABS-KEY%28graphene%29&sort=plf-f&sdt=b&sot=b&sl=23&count=111311&analyzeResults=Analyze+results&xGid=86f1a0b9c91b8a4170>. [Accessed: 23-Apr-2018].
- [5] A. Bonanno *et al.*, "A multipurpose CMOS platform for nanosensing," *Sensors (Switzerland)*, vol. 16, no. 12, pp. 1–15, 2016.
- [6] A. Bonanno, "Tesi di dottorato: Micro-for-Nano," Politecnico di Torino, 2014.
- [7] A. Bonanno, M. Crepaldi, I. Rattalino, P. Motto, D. Demarchi, and P. Civera, "A 0.13 μm CMOS operational schmitt trigger R-to-F converter for nanogap-based nanosensors read-out," *IEEE Trans. Circuits Syst. I Regul. Pap.*, vol. 60, no. 4, pp. 975–988, 2013.
- [8] A. Bonanno *et al.*, "A low-power read-out circuit and low-cost assembly of nanosensors onto a 0.13 μm CMOS micro-for-nano chip," *Proc. 2013 5th IEEE Int. Work. Adv. Sensors Interfaces, IWASI 2013*, pp. 125–130, 2013.
- [9] A. Bonanno *et al.*, "Low-power 0.13- μm CMOS IC for ZnO-nanowire assembly and nanowire-based UV sensor interface," *IEEE Sens. J.*, vol. 15, no. 8, pp. 4203–4212, 2015.
- [10] R. E. Fernandez, A. Rohani, V. Farmehini, and N. S. Swami, "Review: Microbial analysis in dielectrophoretic microfluidic systems," *Anal. Chim. Acta*, vol. 966, pp. 11–33, 2017.
- [11] C. Carati, "Applicazione per l' interfacciamento di nanostrutture con

- tecnologie CMOS-compatibili,” Politecnico di Torino, 2016.
- [12] C. M. Pandey *et al.*, “Microfluidics Based Point-of-Care Diagnostics,” vol. 1700047, pp. 1–11, 2018.
- [13] R. Luttge, *Nano- and microfabrication for industrial and biomedical applications*. 2016.
- [14] M. J. Madou, *Fundamentals of microfabrication: the science of miniaturization*. CRC Press, 2002.
- [15] M. J. Madou, *Fundamentals of microfabrication and nanotechnology: Manufacturing techniques for microfabrication and nanotechnology*, Third edit. CRC Press, 2012.
- [16] S.-J. J. Lee and N. Sundararajan, *Microfabrication for microfluidics*. Artech House, 2010.
- [17] C. A. Mack, *Fundamental principles of optical lithography: the science of microfabrication*. John Wiley & Sons Ltd, 2012.
- [18] H. J. Levinson, *Principles of Lithography*. SPIE (Society of Photo-optical Instrumentation Engineers), 2005.
- [19] L. Prati and A. Villa, *Gold catalysis: preparation, characterization, and applications*. .
- [20] O. Geschke, H. Klank, and P. Telleman, *Microsystem engineering of lab-on-a-chip devices*. Wiley-VCH, 2004.
- [21] Y. Wang, F. Xie, S. Ma, and L. Dong, “Review of surface profile measurement techniques based on optical interferometry,” *Opt. Lasers Eng.*, vol. 93, no. February, pp. 164–170, 2017.
- [22] Y. Xu, X. Xie, Y. Duan, L. Wang, Z. Cheng, and J. Cheng, “A review of impedance measurements of whole cells,” vol. 77, pp. 824–836, 2015.
- [23] C. Páez-Avilés *et al.*, “Combined dielectrophoresis and impedance systems for bacteria analysis in microfluidic on-chip platforms,” *Sensors (Switzerland)*, vol. 16, no. 9, 2016.
- [24] T. Sun and H. Morgan, “Single-cell microfluidic Impedance cytometry: A review,” *Microfluid. Nanofluidics*, vol. 8, no. 4, pp. 423–443, 2010.
- [25] K. C. Cheung *et al.*, “Microfluidic impedance-based flow cytometry,” *Cytom. Part A*, vol. 77, no. 7, pp. 648–666, 2010.
- [26] J. Posseckardt, C. Schirmer, A. Kick, K. Rebatschek, T. Lamz, and M. Mertig, “Monitoring of *Saccharomyces cerevisiae* viability by non-Faradaic impedance spectroscopy using interdigitated screen-printed platinum electrodes,” vol. 255, pp. 3417–3424, 2017.

- [27] H. (Cytologist) Feldmann and P. Branduardi, *Yeast: molecular and cell biology*. Wiley-Blackwell, 2012.
- [28] A. Adami, C. Ressa, C. Collini, S. Pedrotti, and L. Lorenzelli, "Development of an integrated electrochemical system for in vitro yeast viability testing," *Biosens. Bioelectron.*, vol. 40, no. 1, pp. 315–322, 2013.
- [29] T. Ribeiro, G. Romestant, J. Depoortere, and A. Paus, "Development, validation, and applications of a new laboratory-scale indirect impedancemeter for rapid microbial control," *Appl. Microbiol. Biotechnol.*, vol. 63, no. 1, pp. 35–41, 2003.
- [30] N. Barrajon, M. Arévalo-Villena, J. Úbeda, and A. Briones, "Enological properties in wild and commercial *Saccharomyces cerevisiae* yeasts: Relationship with competition during alcoholic fermentation," *World J. Microbiol. Biotechnol.*, vol. 27, no. 11, pp. 2703–2710, 2011.
- [31] J. F. Úbeda, M. Chacoñ-Ocaña, P. Díaz-Hellín, H. Ramírez-Pérez, and A. Briones, "Genetic and phenotypic characterization of *Saccharomyces* spp. Strains isolated in distillery plants," *FEMS Yeast Res.*, vol. 16, no. 4, pp. 1–6, 2016.
- [32] Thermo Fisher Scientific Inc, "OxoidSignal Blood Culture System (BC0100) - Product Detail." [Online]. Available: http://www.oxoid.com/UK/blue/prod_detail/prod_detail.asp?pr=BC0100. [Accessed: 05-Jun-2018].
- [33] J. Claudel, M. Nadi, O. El Mazria, D. Kourtiche, and V. Nancy, "High reliability Microfluidic biosensor for single cell impedance cytometry," no. Umr 7198, pp. 8–12, 2017.
- [34] J. J. Liu, H. Li, F. Zhang, X. Li, L. Wang, and Y. Chen, "Online impedance monitoring of yeast cell culture behaviors," *Microelectron. Eng.*, vol. 88, no. 8, pp. 1711–1713, 2011.